Final Project Report
Development of a dispersion optimized FDTD solver for time dependent numerical simulation of integrated optical components

Hossam Ahmed AbdAllah

June 2001

Abstract

A dispersion optimized finite difference time domain(FDTD) solver for time dependent numerical simulation of integrated optical components is developed. A normalized form of Maxwell's equations is derived and is shown to be efficient for the units of the simulated structures in terms of micrometers for the space and femto seconds for the time. Different finite difference time domain(FDTD) schemes were analyzed and a fourth order one was implemented. A normalized form of the Berenger perfectly matched layer(PML) absorbing boundary conditions(ABCs) is derived. Optimizing and extending the PML-ABCs to model waveguide problems is presented. Among different excitation techniques that are used to introduce input fields to the FDTD lattice, we developed and implemented a one-sided total field/scattered-field (TF/SF) formulation. The developed tool was used to simulate a number of integrated optics structures. The implementation of this tool was done in the Prometheus program, a software program of Kymata.

Contents

1 Introduction **2**

2 Preliminaries **4**
- 2.1 Maxwell's Equations . . . 4
- 2.2 Boundary Conditions at a Dielectric Interface . . . 4
- 2.3 Normalized Maxwell's Equations . . . 5
- 2.4 TE and TM Normalized Maxwell Equations . . . 6

3 High Order FDTD Schemes **7**
- 3.1 Differential Equations and Difference Notations in 1D . . . 7
- 3.2 The Yee Scheme . . . 9
- 3.3 A Fourth Order Explicit Scheme . . . 9
- 3.4 A Fourth Order Implicit Scheme with Optimized LU Decomposition . . . 10
- 3.5 Accuracy of Different FDTD Schemes . . . 12
- 3.6 Dispersion of Different FDTD Schemes . . . 14
- 3.7 Conclusion . . . 18

4 Absorbing Boundary Conditions: The Perfectly Matched Layers **19**
- 4.1 How Does the PML Work? . . . 19
- 4.2 Two Dimensional Berenger PML . . . 20
- 4.3 Two Dimensional Unsplit PML Formulation . . . 22
- 4.4 Choice of the PML Parameters . . . 24
- 4.5 Numerical and Implementation Concerns for the PML and Unsplit PML Formulations 26
- 4.6 Conclusion . . . 27

5 Sources in FDTD Simulation **28**
- 5.1 Hard Source Excitation . . . 28
- 5.2 Excitation Through PMLs Window . . . 28
- 5.3 Transparent Source Excitation . . . 30
- 5.4 One-Sided vs. Two-sided Total-Field/Scattered-Field Formulation . . . 32
- 5.5 Conclusion . . . 37

6 Application of FDTD to 2D Integrated Optical Devices **38**
- 6.1 Waveguides . . . 38
- 6.2 Directional Coupler . . . 40
- 6.3 Conclusion . . . 41

7 Conclusions and Recommendations **42**

Chapter 1

Introduction

There are different wave modeling techniques that are successfully used in modeling integrated optics structures. Finite difference time domain (FDTD), Fourier transform- beam propagation method (FT-BPM), finite difference-beam propagation method (FD-BPM), and finite element beam propagation method (FE-BPM) are the most popular and useful techniques for the simulation of integrated optics structures.

FT-BPM, FD-BPM, or FE-BPM were developed for the case of weakly guiding structures where the use of the paraxial approximation and the neglection of any back reflections offer solutions in the frequency-domain. These characteristics limited the use of these methods when these assumptions are no longer valid.

The FDTD method overcomes the disadvantages of the previous methods. In simulating guided-wave optics the method became increasingly popular due to its attractive features such as ease of implementation and full-wave simulation including multiple reflections and radiation.

The first FDTD algorithm as proposed by Yee[**?**] provides a simple and efficient direct solution to the Maxwell's equations. To insure the numerical accuracy of the Yee scheme the size of the spatial finite difference step size has to be smaller than the wavelength by a certain factor, 10 to 20 points per wavelength (PPW). Alternatively higher order FDTD schemes [**?**] may be used.

In order to avoid nonphysical reflections from a finite computational window when simulating an open problem, absorbing boundary conditions (ABCs) need to be implemented at the edges of the computational window. The ABCs must be able to absorb waves that impinge on the boundaries regardless of the polarization and the incident angles.

Berenger's perfectly matched layer (PML) ABCs [**?**] offer excellent absorbing performance in FDTD applications. It is based on covering the computational window with another region with different (artificial) material properties such that a wave propagating from the interior will not be reflected and at the same time will decay in the PML region.

Among the other ABCs, unsplit PML [**?**], [**?**] or using electric the displacement instead of the electric field and the uniaxial PML (UPML) [**?**], [**?**] are the most successful extensions to Berenger PML. The unsplit PML and UPML have the advantages of offering possibilities of simulating structures filled with more complex materials in a straightforward way. Nevertheless, the computation cost increases due to the introduction of new field components.

While implementation of sources is a straightforward procedure in many FDTD simulations, certain applications require more complicated procedures. The complications come from the requirements to terminate waveguides that are extended beyond the grid boundaries. All excitation techniques intend to couple the exact incident power to the FDTD grid, allow back reflected waves to pass through the excitation position, to avoid the interaction between simulated sources and the ABCs, and, finally, to decrease the load on the ABCs.

Different techniques can be used to excite waveguide structures. A popular method is the

use of the total-field/scattered-field (TF/SF) method [**?**]. By introducing the TF/SF formulation, the simulation domain will be divided into three domains: the total-field domain, the scattered field domain, and the PML domain. The SF domain offers information about any scattered field meanwhile decreasing the load on ABCs. We developed and used a one sided TF/SF formulation that is suited for waveguide problems. Another possible excitation is to define the incident field at the outer boundary of the PML domain and then allowing this field to propagate and attenuate inside the PML domain. By using the PML's properties the corrected/desired field profile can be recalculated at the inner PML-main domain interface [**?**].

This work reports on developing a time domain simulation tool for simulating integrated optics structures. This includes choosing and implementing a higher order FDTD scheme, PMLs-ABCs, and implementing the TF/SF formulation. This is tool is used to simulate a number of **2D** integrated optic structures.

This report consists of seven chapters arranged as follow. After this chapter introduction. Chapter two introduces normalized Maxwell equations. Chapter three presents different higher order FDTD schemes and the assessment of the accuracy and dispersion of these schemes. Chapter four presents the PMLs-ABCs. Chapter five introduces different techniques that are used in exciting structures. In chapter six we provide visual assessment to the performance of our developed FDTD tool. Chapter seven presents conclusion and recommendations.

Chapter 2

Preliminaries

This chapter introduces a normalized form of Maxwell's equations.

2.1 Maxwell's Equations

Optical fields are time dependent fields and their behavior is fully described by the set of Maxwell equations. Maxwell's equations for the electric field vector $\mathbf{E}$, the electric displacement vector $\mathbf{D}$, the magnetic field vector $\mathbf{H}$, and the magnetic induction vector $\mathbf{B}$ in a region without free charges and currents, filled with linear, isotropic, nondispersive materials with the permittivity ϵ and permeability μ, given in a three dimensional coordinate system are

$$\partial_t \mathbf{D} = \nabla \times \mathbf{H}, \tag{2.1}$$

$$\partial_t \mathbf{B} = -\nabla \times \mathbf{E}, \tag{2.2}$$

$$\nabla \cdot \mathbf{B} = 0 \tag{2.3}$$

$$\nabla \cdot \mathbf{D} = 0 \tag{2.4}$$

$$\mathbf{D} = \epsilon_0 \epsilon_r \mathbf{E}, \tag{2.5}$$

$$\mathbf{B} = \mu_0 \mathbf{H}. \tag{2.6}$$

where ϵ_0 is the permittivity of the free space, ϵ_r is the relative dielectric constant, and μ_0 is the permeability of the free space, assuming non-magnetic materials.

Traditionally, most of simulations consider only $\mathbf{E}$ and $\mathbf{H}$ as explicit unknowns: $\epsilon_0 \epsilon_r \partial_t \mathbf{E} = \nabla \times \mathbf{H}$, $\mu_0 \partial_t \mathbf{H} = -\nabla \times \mathbf{E}$. We will call this set of basic equations the $\mathbf{EH}$ set.

2.2 Boundary Conditions at a Dielectric Interface

In inhomogeneous media filled with different dielectric materials, the four vectors $\mathbf{D}$, $\mathbf{E}$, $\mathbf{H}$, and $\mathbf{B}$ have to satisfy certain boundary conditions. Fig.(2.1) shows a simple structure consisting of two media with different dielectric properties.

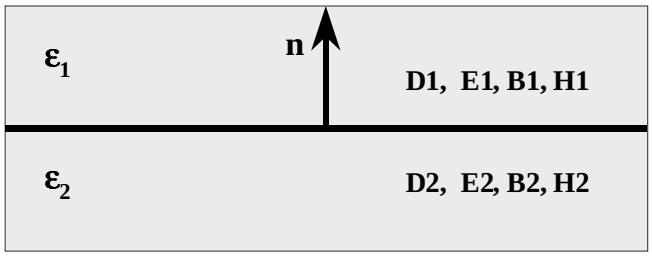

Fig.(2.1) Discontinuity in material properties

When surface charges and surface currents are absent, the boundary conditions at the dielectric interface reduce to [?]:

- The tangential components of the electric field are continuous.

$$\mathbf{n} \times \mathbf{E_1} = \mathbf{n} \times \mathbf{E_2}, \tag{2.7}$$

- The tangential components of the magnetic field are continuous.

$$\mathbf{n} \times \mathbf{H_1} = \mathbf{n} \times \mathbf{H_2}, \tag{2.8}$$

- The normal component of the electric displacement is continuous.

$$\mathbf{n} \cdot \mathbf{D_1} = \mathbf{n} \cdot \mathbf{D_2}, \tag{2.9}$$

- The normal component of the magnetic induction is continuous.

$$\mathbf{n} \cdot \mathbf{B_1} = \mathbf{n} \cdot \mathbf{B_2}. \tag{2.10}$$

2.3 Normalized Maxwell's Equations

For two reasons we chose to work with normalized Maxwell's equations. The first reason is the difference in order of magnitude between the **E** and **H** fields which may lead to loss of accuracy and round off errors when discretizing the Maxwell's equations. The second reason is related to the units of the problem in terms of micrometers for the space and femto seconds for the time, and the formulation of the absorbing boundary conditions (ABCs). Working with these units requires working with very large or very small numbers for all constants such as ϵ_0 and μ_0.

We introduce the normalized fields $\bar{\mathbf{E}}$ as

$$\bar{\mathbf{E}} = \sqrt{\frac{\epsilon_0}{\mu_0}}\mathbf{E}, \tag{2.11}$$

With the speed of light in free space $c_0 = \frac{1}{\sqrt{\epsilon_0 \mu_0}}$, the normalized **EH** set is, removing the hat above the normalized fields,

$$\epsilon_r \partial_t \mathbf{E} = c_0 \nabla \times \mathbf{H}, \tag{2.12}$$

$$\partial_t \mathbf{H} = -c_0 \nabla \times \mathbf{E}, \tag{2.13}$$

2.4 TE and TM Normalized Maxwell Equations

The **EH** set in a three dimensional rectangular coordinate system (x, y, z) is

$$\partial_t H_x = c_0 \left(\partial_z E_y - \partial_y E_z\right) \tag{2.14}$$

$$\partial_t H_y = c_0 \left(\partial_x E_z - \partial_z E_x\right), \tag{2.15}$$

$$\partial_z H_z = c_0 \left(\partial_y E_x - \partial_x E_y\right), \tag{2.16}$$

$$\epsilon_r \partial_t E_x = c_0 \left(\partial_y H_z - \partial_z H_y\right), \tag{2.17}$$

$$\epsilon_r \partial_t E_y = c_0 \left(\partial_z H_x - \partial_x H_z\right), \tag{2.18}$$

$$\epsilon_r \partial_t E_z = c_0 \left(\partial_x H_y - \partial_y H_x\right). \tag{2.19}$$

In a 2D setting, assuming that both the fields and the dielectric structure are constant along the $y-$direction, the equations (2.14)-(2.19) decouple into two sets. One set is constituted by electromagnetic fields with vanishing components E_x, E_z, H_y.

$$\epsilon_r \partial_t E_y = c_0 \left(\partial_z H_x - \partial_x H_z\right), \tag{2.20}$$

$$\partial_t H_x = c_0 \partial_z E_y, \tag{2.21}$$

$$\partial_t H_z = -c_0 \partial_x E_y. \tag{2.22}$$

These fields are called the TE fields. The second set has vanishing E_y, H_x, H_z components.

$$\partial_t H_y = -c_0 \left(\partial_z E_x - \partial_x E_z\right), \tag{2.23}$$

$$\epsilon_r \partial_t E_x = -c_0 \partial_z H_y, \tag{2.24}$$

$$\epsilon_r \partial_t E_z = c_0 \partial_x H_y. \tag{2.25}$$

These fields are called TM fields. The two sets are completely decoupled; there is no common field vector component. Therefore TE and TM fields constitute two possible classes of solutions for two dimensional electromagnetic problems.

If the medium is inhomogeneous along the x-direction, then boundary conditions at material interfaces imply that E_y, $\frac{\partial E_y}{\partial x}$, and H_z are continuous for TE fields. For TM fields H_y and E_z are continuous while $\frac{\partial H_y}{\partial x}$ is not.

Chapter 3

High Order FDTD Schemes

It is well known that the original FDTD scheme is dispersive, less accurate, and computational expensive. In this chapter we shall show explicitly how severe the dispersion of the scheme is. Firstly, by visual assessment through looking at higher order FDTD schemes and comparing the accuracy of these scheme and the original one. Secondly, by applying a model problem to formally check the dispersion limitation of the original and the higher order schemes.

We derive a simple algorithm to perform the LU decomposition specifically for a certain implicit fourth order accurate FDTD scheme. The new algorithm requires less number of operations to perform the LU decomposition.

3.1 Differential Equations and Difference Notations in 1D

We introduce and derive some notations for the finite differences that will be used for the FDTD schemes under consideration. For simplicity we consider a one dimensional finite difference notation. We apply and analyze different FDTD schemes in **1D** and then extend the implementation of the most appropriate scheme to **2D**.

The TE field equations in **1D** are

$$\epsilon_r \partial_t E_y = c_0 \partial_z H_x, \tag{3.1}$$

$$\partial_t H_x = c_0 \partial_z E_y. \tag{3.2}$$

As shown in fig.(3.1) and as proposed by Yee [**?**], the discretization points for E_y and H_y are interleaved in space and time.

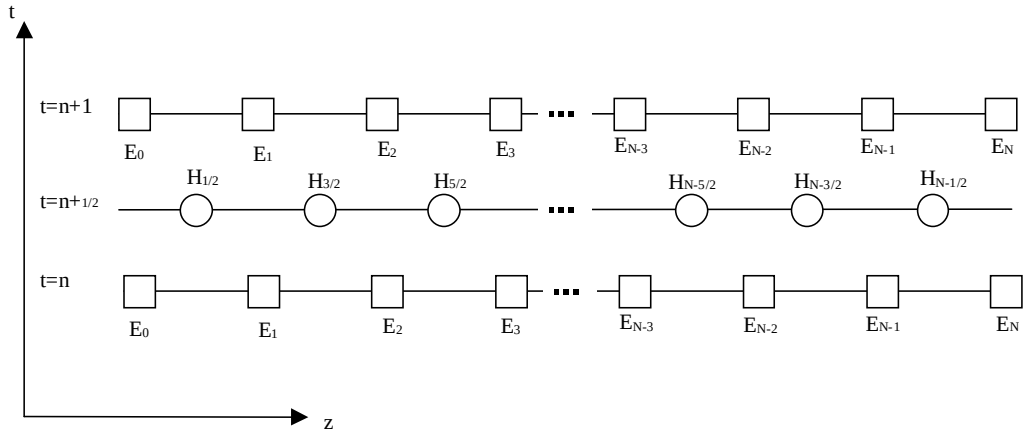

Fig.(3.1) Position of discretization points in a 1D grid, circles are for E_y and squares are for H_x for TE fields

We present notations for approximating the first and second derivatives in space or time at certain position using the neighboring points. We denote by ζ either E_y or H_x. We assume equidistant discretization with the step size Δz in the z-direction and the time step size Δt and define $\zeta_i^n = \zeta(n\Delta t, i\Delta z)$. δ_z and δ_z^2 are the approximations to the first and second derivative with respect to z, respectively. We differentiate between two grids. The first grid is the staggered grid in which E_y and H_x are located in space as in fig.(3.1), the second grid is the non-staggered grid in which E_y and Hy are located at the same space and time positions.

For the staggered grid we define the following finite difference expressions

$$\delta_z \zeta_{i+1/2}^n = \frac{\zeta_{i+1}^n - \zeta_i^n}{\Delta z} + O(\Delta z)^2 \tag{3.3}$$

$$\delta_z \zeta_i^{n+\frac{1}{2}} = \frac{\zeta_{i+1/2}^{n+\frac{1}{2}} - \zeta_{i-1/2}^{n+\frac{1}{2}}}{\Delta z} + O(\Delta z)^2 \tag{3.4}$$

$$\delta_t \zeta_i^{n+\frac{1}{2}} = \frac{\zeta_i^{n+1} - \zeta_i^n}{\Delta t} + O(\Delta t)^2 \tag{3.5}$$

$$\delta_t \zeta_{i+\frac{1}{2}}^n = \frac{\zeta_{i+\frac{1}{2}}^{n+\frac{1}{2}} - \zeta_{i+\frac{1}{2}}^{n-\frac{1}{2}}}{\Delta t} + O(\Delta t)^2 \tag{3.6}$$

For higher order FDTD schemes we use also the following non-symmetric stencils, for the second order spatial derivatives

$$\delta_z^2 \zeta_{i+1/2}^n = \frac{\zeta_{i-1}^n - 2\zeta_i^n + \zeta_{i+1}^n}{(\Delta z)^2} + O(\Delta z)^2 \tag{3.7}$$

$$\delta_z^2 \zeta_i^{n+\frac{1}{2}} = \frac{\zeta_{i-3/2}^{n+\frac{1}{2}} - 2\zeta_{i-1/2}^{n+\frac{1}{2}} + \zeta_{i+1/2}^{n+\frac{1}{2}}}{(\Delta z)^2} + O(\Delta z)^2 \tag{3.8}$$

and for non-staggered grid

$$\delta_z \zeta_i^n = \frac{\zeta_{i+1}^n - \zeta_{i-1}^n}{2\Delta z} + O(\Delta z)^2 \tag{3.9}$$

$$\delta_t \zeta_i^n = \frac{\zeta_i^{n+1} - \zeta_i^{n-1}}{\Delta t} + O(\Delta t)^2 \tag{3.10}$$

$$\delta_z^2 \zeta_i^n = \frac{\zeta_{i-1}^n - 2\zeta_i^n + \zeta_{i+1}^n}{(\Delta z)^2} + O(\Delta z)^2. \tag{3.11}$$

The minor problem or disadvantage when using staggered grids is the need to perform post-processing calculation/interpolation to evaluate field values at the same spatial and temporal positions. These requirements complicate the simplicity of the FDTD scheme and require additional computation time and programming effort.

3.2 The Yee Scheme

Yee formulated the first FDTD scheme [?] on a staggered grid using a second order accurate approximation to the spatial and time derivatives. We will refer to it as Yee(2,2), where (2,2) refers to the order of accuracy in time and space, respectively. For the **1D** TE fields given by equations 3.1 and 3.2, the Yee(2,2) scheme will have the form

$$\epsilon_r|_i \; \delta_t E_y|_i^{n+\frac{1}{2}} = c_0 \; \delta_z H_x|_i^{n+\frac{1}{2}} \,, \tag{3.12}$$

$$\delta_t H_x|_{i+\frac{1}{2}}^{n} = c_0 \; \delta_z E_y|_{i+\frac{1}{2}}^{n+\frac{1}{2}} \,. \tag{3.13}$$

Equations 3.12 and 3.13 are rewritten to yield explicit expressions for E_y^{n+1} given $H_x^{n+\frac{1}{2}}$ and E_y^n and for $H_x^{n+\frac{1}{2}}$ given E_y^n and $H_x^{n-\frac{1}{2}}$. Thus, from initial field distribution E_y^0, the algorithm can advance alternatingly E_y and H_x in time.

The Yee(2,2) algorithm is a conditionally stable algorithm which means that the time and space steps must satisfy certain criteria. In **1D** the stability criteria is

$$\triangle t \leq \frac{\triangle z}{c_0} \tag{3.14}$$

3.3 A Fourth Order Explicit Scheme

The second FDTD scheme we consider is an explicit fourth order accurate scheme in space and second order in time [?]. We refer to it as Explicit(2,4). Due to the long stencil employed by the scheme, a one sided fourth order accurate approximation is required to approximate the derivatives at the boundary points. The difference notations for the fourth order scheme will have the form

$$\delta_z \zeta_{i+1/2}^n = \frac{1}{24}\left(\zeta_{i-1}^n - 27\zeta_i^n + 27\zeta_{i+1}^n - \zeta_{i+2}^n\right), \tag{3.15}$$

$$\delta_z \zeta_i^{n+\frac{1}{2}} = \frac{1}{24}\left(\zeta_{i-3/2}^{n+\frac{1}{2}} - 27\zeta_{i-1/2}^{n+\frac{1}{2}} + 27\zeta_{i+1/2}^{n+\frac{1}{2}} - \zeta_{i+3/2}^{n+\frac{1}{2}}\right), \tag{3.16}$$

and for the first point and last point from the boundary a one sided fourth order approximation is used

$$\delta_z \zeta_{1/2}^n = \frac{1}{24}\left(-22\zeta_0^n + 17\zeta_1^n + 9\zeta_2^n - 5\zeta_3^n + \zeta_4^n\right), \tag{3.17}$$

$$\delta_z \zeta_{N-1/2}^n = \frac{1}{24}\left(22\zeta_N^n - 17\zeta_{N-1}^n - 9\zeta_{N-2}^n - 5\zeta_{N-3}^n - \zeta_{N-4}^n\right), \tag{3.18}$$

$$\delta_z \zeta_1^{n+\frac{1}{2}} = \frac{1}{24}\left(-23\zeta_{1/2}^{n+\frac{1}{2}} + 21\zeta_{3/2}^{n+\frac{1}{2}} - 3\zeta_{5/2}^{n+\frac{1}{2}} + \zeta_{7/2}^{n+\frac{1}{2}}\right), \tag{3.19}$$

$$\delta_z \zeta_{N-1}^{n+\frac{1}{2}} = \frac{1}{24}\left(23\zeta_{N-1/2}^{n+\frac{1}{2}} - 21\zeta_{N-3/2}^{n+\frac{1}{2}} + 3\zeta_{N-5/2}^{n+\frac{1}{2}} - \zeta_{N-7/2}^{n+\frac{1}{2}}\right). \tag{3.20}$$

The Explicit scheme remains stable providing the following criteria is satisfied

$$\triangle t \leq \frac{6}{7}\frac{\triangle z}{c_0} \tag{3.21}$$

Due to the mixed order of accuracy of the Explicit(2,4) scheme, $\mathbf{O}(\Delta t)^2 + \mathbf{O}(\Delta z)^4$, either the time step should be a function of the $\mathbf{O}(\Delta z)^2$ or it should be chosen small enough such that the total order of accuracy of the scheme with respect to the spatial discretization remains fourth order and is not reduced to second order. In all situations the Explicit(2,4) scheme introduces better approximations with minimum additional computation cost.

3.4 A Fourth Order Implicit Scheme with Optimized LU Decomposition

The third scheme is an implicit fourth order scheme in space and second order in time [?]. We refer to it as Implicit(2,4). The derivation of the Implicit(2,4) scheme starts with calculating the truncation error to the fourth order when approximating the first derivatives. This leads to

$$\delta_z \zeta_{i+1/2}^{n+\frac{1}{2}} = (1 + \frac{(\triangle z)^2}{24}\, \partial_z^2\big|_{i+1/2}) \partial_z \zeta_{i+1/2}^{n+\frac{1}{2}} + O(\triangle z)^4, \tag{3.22}$$

and by introducing a discrete approximation to the operator $\partial_z^2\big|_{i+1/2}$ by $\delta^2\big|_{i+1/2}$ as given in 3.11, we obtain

$$\delta_z \zeta_{i+1/2}^{n+\frac{1}{2}} = (1 + \frac{(\triangle z)^2}{24}\delta^2)\, \frac{\partial \zeta}{\partial z}\Big|_{i+1/2}^{n+\frac{1}{2}} + O(\triangle z)^4. \tag{3.23}$$

To express the first order derivatives $\delta_z \zeta_{i+1/2}^{n+\frac{1}{2}}$ explicitly in terms of the field values of the neighboring grid points, the scheme requires the inversion of a matrix which is tridiagonal except at the first and last rows. This because of the need to use one sided fourth order accurate implicit approximations to the derivatives at the first and last points at the boundary.

The inversion of the tridiagonal matrix can be replaced by decomposing the matrix using the LU decomposition. This process will be done twice per each simulation. Once when approximating the first derivatives of fields at the half grid points and once for those at the main grid points. Performing the LU decomposition requires 5N operations and L and U will be bidiagonal matrices, except at a few rows, with one of them containing ones on the diagonal [?]. Therefore it is possible to store the results of the LU decomposition using only 3 vectors each of size N.

We derive a simple and optimized algorithm that can be used to perform the LU decomposition specifically for the discretized matrix from the Implicit(2,4) scheme. The discretized matrix of the system in 3.22 will have the form, dropping the time dependence notation for the moment

$$\begin{bmatrix} 26 & -5 & 4 & -1 & 0 & . & 0 \\ 1 & 22 & 1 & 0 & 0 & . & 0 \\ 0 & 1 & 22 & 1 & 0 & . & 0 \\ . & . & . & . & . & . & . \\ 0 & . & . & 0 & 1 & 22 & 1 \\ 0 & . & . & -1 & 4 & -5 & 26 \end{bmatrix} \begin{bmatrix} \partial_z\zeta|_{1/2} \\ \partial_z\zeta|_{3/2} \\ \partial_z\zeta|_{5/2} \\ . \\ \partial_z\zeta|_{N-3/2} \\ \partial_z\zeta|_{N-1/2} \end{bmatrix} = \frac{24}{\triangle z} \begin{bmatrix} \zeta_1 - \zeta_0 \\ \zeta_2 - \zeta_1 \\ \zeta_3 - \zeta_2 \\ . \\ \zeta_{N-1} - \zeta_{N-2} \\ \zeta_N - \zeta_{N-1} \end{bmatrix} \tag{3.24}$$

Performing one time gauss elimination to the first and last rows only results in

$$\begin{bmatrix} 0 & 1 & 0 & 0 & 0 & . & 0 \\ 1 & 22 & 1 & 0 & 0 & . & 0 \\ 0 & 1 & 22 & 1 & 0 & . & 0 \\ . & . & . & . & . & . & . \\ 0 & . & . & 0 & 1 & 22 & 1 \\ 0 & . & . & 0 & 0 & 1 & 0 \end{bmatrix} \begin{bmatrix} \partial_z\zeta|_{1/2} \\ \partial_z\zeta|_{3/2} \\ \partial_z\zeta|_{5/2} \\ . \\ \partial_z\zeta|_{N-3/2} \\ \partial_z\zeta|_{N-1/2} \end{bmatrix} = \frac{24}{\triangle z} \begin{bmatrix} b_1 \\ \zeta_2 - \zeta_1 \\ \zeta_3 - \zeta_2 \\ . \\ \zeta_{N-1} - \zeta_{N-2} \\ b_N \end{bmatrix} \tag{3.25}$$

with

$$b_1 = \frac{1}{(24)^2}(27(\zeta_2 - \zeta_1) - (\zeta_3 - \zeta_0)) \tag{3.26}$$

and

$$b_N = \frac{1}{(24)^2}(27(\zeta_{N-2} - \zeta_{N-1}) - (\zeta_{N-3} - \zeta_N)) \tag{3.27}$$

When simulating TE fields, the process of solving the linear system will be repeated twice for **1D** problems, four times for **2D** with PML-ABCs, see chapter four, and much more in **3D**. For a large number of time steps, the computation time of the Implicit(2,4) scheme may limit the use of the scheme for simulating large structures. Hence, any optimization to the LU decomposition process will effectively reduce the total computation time.

Rather than performing the LU decomposition on the systems in 3.24 or 3.25 as proposed in [**?**], we eliminate $\partial_z\zeta|_{3/2}$ and $\partial_z\zeta|_{N-3/2}$ from 3.25 and perform the LU decomposition. The resulting system has the form

$$\begin{bmatrix} 1 & 1 & 0 & 0 & 0 & . & 0 \\ 0 & 22 & 1 & 0 & 0 & . & 0 \\ 0 & 1 & 22 & 1 & 0 & . & 0 \\ 0 & 0 & 1 & 22 & 1 & . & 0 \\ . & . & . & . & . & . & . \\ 0 & . & 1 & 22 & 1 & 0 & 0 \\ 0 & . & 0 & 1 & 22 & 1 & 0 \\ 0 & . & 0 & 0 & 1 & 22 & 0 \\ 0 & . & 0 & 0 & 0 & 1 & 1 \end{bmatrix} \begin{bmatrix} \partial_z\zeta|_{1/2} \\ \partial_z\zeta|_{5/2} \\ \partial_z\zeta|_{7/2} \\ \partial_z\zeta|_{9/2} \\ . \\ \partial_z\zeta|_{N-9/2} \\ \partial_z\zeta|_{N-7/2} \\ \partial_z\zeta|_{N-5/2} \\ \partial_z\zeta|_{N-1/2} \end{bmatrix} = \frac{24}{\triangle z} \begin{bmatrix} b_1 \\ b_2 \\ b_3 \\ \zeta_4 - \zeta_3 \\ . \\ \zeta_{N-4} - \zeta_{N-5} \\ b_{N-2} \\ b_{N-1} \\ b_N \end{bmatrix} \tag{3.28}$$

with

$$b_2 = (\zeta_2 - \zeta_1) - 22b_1 \tag{3.29}$$

$$b_3 = (\zeta_3 - \zeta_2) - b_1 \tag{3.30}$$

$$b_{N-2} = (\zeta_{N-3} - \zeta_{N-2}) - b_N \tag{3.31}$$

$$b_{N-1} = (\zeta_{N-2} - \zeta_{N-1}) - 22b_N \tag{3.32}$$

The LU decomposition of the matrix in 3.28 will result in two matrices L and U on the following form

$$L * U = \begin{bmatrix} 1 & 0 & 0 & 0 & . & 0 & 0 \\ 0 & 1 & 0 & 0 & . & 0 & 0 \\ 0 & a_1 & 1 & 0 & . & 0 & 0 \\ 0 & 0 & a_2 & 1 & . & 0 & 0 \\ . & . & . & . & . & . & . \\ 0 & 0 & 0 & . & a_{p-1} & 1 & 0 \\ 0 & 0 & 0 & . & 0 & a_p & 1 \end{bmatrix} \begin{bmatrix} 1 & 1 & 0 & 0 & . & 0 & 0 \\ 0 & 1/a_1 & 1 & 0 & . & 0 & 0 \\ 0 & 0 & 1/a_2 & 1 & . & 0 & 0 \\ 0 & 0 & 0 & 1/a_3 & . & 0 & 0 \\ . & . & . & . & . & . & . \\ 0 & 0 & 0 & . & . & 1/a_p & . \\ 0 & 0 & 0 & 0 & . & 0 & 1 \end{bmatrix} \tag{3.33}$$

The values of a_i can be calculated using the simple expression

$$a_1 = \frac{1}{22}, \qquad a_i = \frac{1}{22 - a_{i-1}}, \qquad i = 2, 3, 4, ..., p \tag{3.34}$$

Due to the round off error and the precision accuracy, we found that $a_i \approx a_6$ for $i \succ 6$ with error less than 10^{-15}. This suggest to store only the values a_i, $i = 1.2, ..., 6$.

This not only reduces the number of operations and the storage requirements to perform the LU decomposition but also reduces the number of operations to solve the linear system using the above LU formulation. The algorithm used to solve the linear system $LUX = b$ will be carried out by solving $LY = b$ with $Y = UX$. For the first system the algorithm will have the form

$$\begin{aligned} Y_1 &= b_1, \quad Y_2 = b_2 \\ Y_i &= b_i - a_{i-2} * Y_{i-1} \qquad i = 3, 4, 5, ..., p+2 \end{aligned} \tag{3.35}$$

and for solving $Y = UX$

$$\begin{aligned} X_{p+2} &= Y_{p+2}, \qquad X_{p+1} = Y_{p+1} * a_p \\ X_i &= (Y_i - X_{i+1}) * a_{i-1}, \quad i = p-1, p-2, ..., 2 \\ X_1 &= Y_1 - X_2 \end{aligned} \tag{3.36}$$

Performing a simulation in **1D** using the Implicit(2,4) scheme requires performing the LU decomposition once and storing the resulting matrices. For each time step the process of solving the linear system will be repeated twice, once when solving for the E_y field and the second when solving for the H_x field, assuming TE polarization. The implicit scheme is explicit in time and there is no stability limitatoin for the time step.

3.5 Accuracy of Different FDTD Schemes

We confirm the second and fourth order of accuracy with respect to the spatial discretization of the previously presented FDTD schemes in one dimension, similarly the extension in two dimensions.

The following results are obtained for a sinusoidal wave with wavelength $1.0\mu m$ propagating in free space in the positive $z-$direction over a distance of $10\mu m$. For $\epsilon_r = 1$, angular frequency ω, and wavenumber k, an exact solution of the **1D** TE field equations will have the form

$$E_y(z,t) = \sin(\omega t - kz), \tag{3.37}$$

$$H_x(z,t) = -\sin(\omega t - kz), \tag{3.38}$$

which represents a wave traveling in the $+z$-direction with speed c_0. This solution satisfies the **1D** equations provided that the following dispersion relation is satisfied

$$k = \frac{\omega}{c_0}. \tag{3.39}$$

The wave is introduced into the **1D** grid as a hard source; details and different excitation techniques are explained in chapter five, at the left boundary and on the right boundary a PML of thickness 8 cells was used; details about the PMLs-ABCs are explained in chapter four. In order to avoid the influence of the BCs on the assessment of the accuracy of the different schemes, the wave will travel till it reaches the right boundary and the time it takes to do so can easily be estimated. This total time for the simulation and the time step were fixed for all the schemes and for all the simulations. The spatial step size $\triangle z$ and the number of grid points N were chosen as function of the wavelength, $\triangle z = \frac{\lambda}{PPW}$, where PPW is the number of points per wavelength which was chosen to be $[5, 10, 15, ..., 40]$.

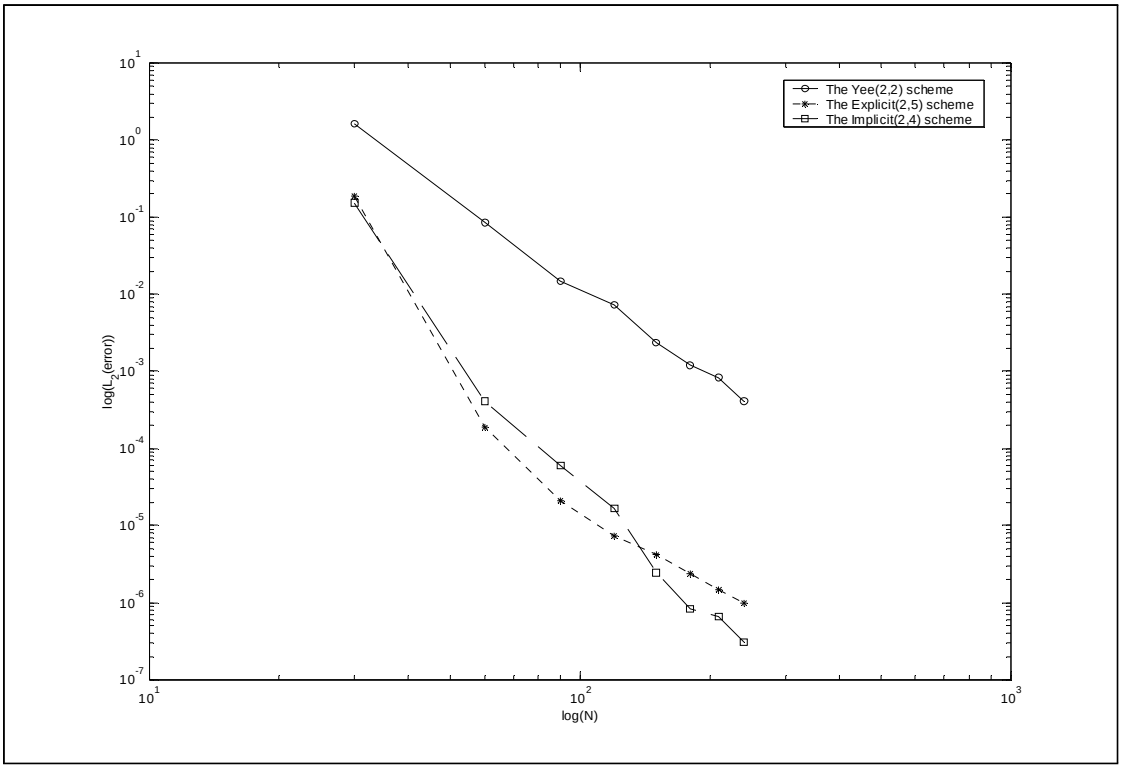

Fig.(3.2) L_2 norm of the difference between the numerical and exact values for E_y field at the last time step using the Yee(2,2), Explicit(2,4), and Implicit(2,4) scheme at different points per wavelength, $\triangle t$ was not a function of $(\triangle x)^2$ as it should be.

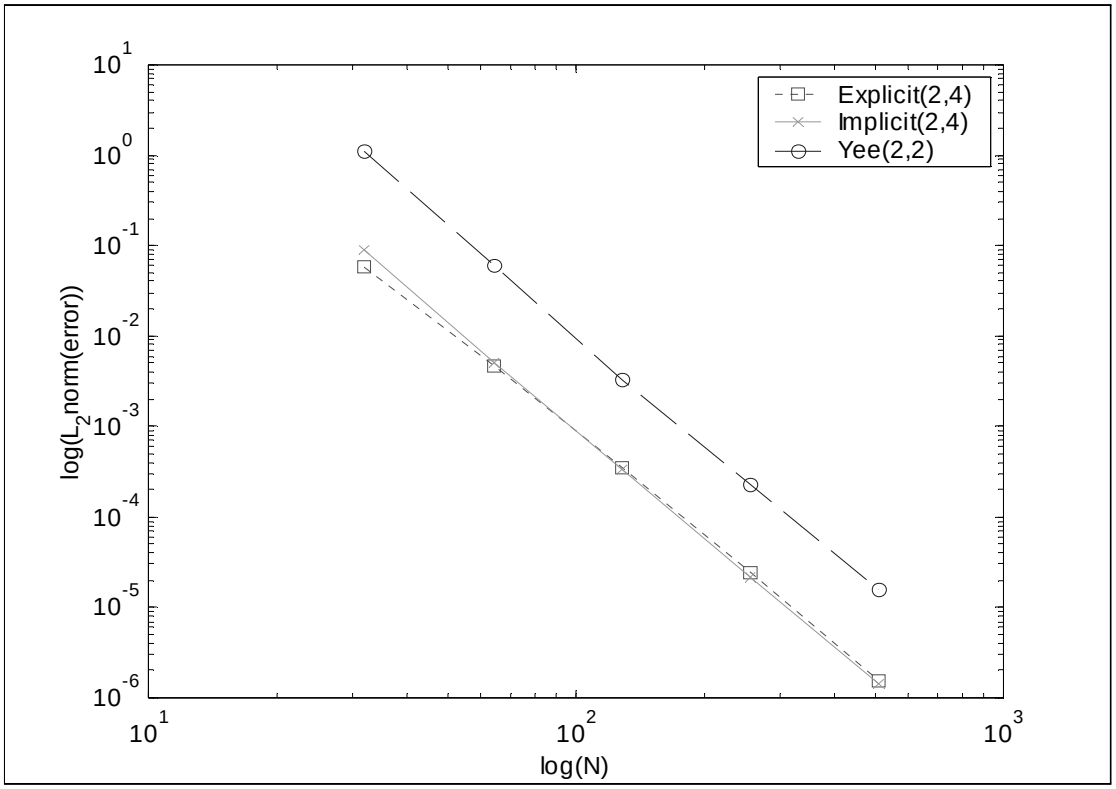

Fig.(3.3) L_2 norm of the difference between the numerical and exact values for Ey field at the last time step using the Yee(2,2), Explicit(2,4), and Implicit(2,4) scheme at different points per wavelength.

Fig.(3.2) shows the L_2 norm calculated for the E_y field at the last calculated time step where the increment of the time step was chosen to a function of be $(\triangle x)^2$. The Explicit(2,4) and Implicit(2,4) schemes present a substantial improvement compared to the Yee(2,2) scheme even when the increment of $\triangle t$ was not a function of $(\triangle x)^2$ as can be seen from fig.(3.3).

The Implicit(2,4) scheme does not introduce a substantial improvement compared to the Explicit(2,4) except its usefulness in allowing arbitrary time steps. Nevertheless this can be considered an disadvantage since coarser time steps result in reduction of the overall order of accuracy of the scheme. Therefore, we choose to focus our implementation and analysis on the Explicit(2,4) scheme.

3.6 Dispersion of Different FDTD Schemes

Dispersion of the original Yee algorithm is one of the main problems which limits the use of the algorithm in many applications. The dispersion can be seen as an error in phase velocity due to the difference in speed between the real wave and the simulated wave. The error accumulates as the electromagnetic wave advances in the FDTD lattice.

A one dimensional model problem is used to assess the dispersion of the different FDTD schemes under consideration. It can be extended to 2D problems in a straightforward way. It is based on approximating the eigenvalues of a solution of the scalar wave equation of either E_y or H_x.

We combine eq. 3.1 and eq. 3.2 into the following wave equation, assuming propagation in free

space, $\epsilon_r = 1$,

$$(\partial_{zz} - \frac{1}{c_0^2}\partial_{tt})E_y(z,t) = 0. \tag{3.40}$$

$E_y(z,t)$ is introduced as a sum of N_o orthogonal eigenfunctions of the form

$$E_y(z,t) = \sum_{n=1}^{N_o} a_n \cos(k_n z)\cos(\omega_n t), \tag{3.41}$$

leading to an initial condition, assuming $a_n = 1$

$$E_y(z,0) = \sum_{n=1}^{N_o} \cos(k_n z). \tag{3.42}$$

The values of k_n have the form

$$k_n = (n + \frac{1}{2})\pi, \tag{3.43}$$

and the values of z at the left and right edge were chosen such that the $E_y(z,t)$ is always zero. For the numerical results presented in this section, the values of n were $1, 2, ..., 50$, z at the left edge was $1\mu m$ and at the right edge $9\mu m$, the time step was chosen to be $0.01fs$ and the simulation was run for 2621.44 fs, 262144 iterations. These numbers were used with both the Yee(2,2) and Explit(2,4) scheme.

$$f(t) = \int_{z_0}^{z_n} E_y(z,t)E(z,0)dz. \tag{3.44}$$

Substituting eq.3.41 and eq. 3.42 in eq. 3.44 $f(t)$ evaluates to

$$f(t) = \sum_{n=1}^{N_o} \cos(\omega_n t). \tag{3.45}$$

A Fourier transform of eq. 3.45 will result in

$$\mathcal{F}[f(t)] = \frac{\pi}{2}\sum_{n=1}^{N_o} \delta(\omega - \omega_n) \tag{3.46}$$

Hence, the idea is to evaluate $f(t)$ numerically on the basis of the discretized field, i.e. as

$$f(t = n \triangle t) = \triangle z \sum_i E_y(z_i, n \triangle t)E(z_i, 0) \tag{3.47}$$

at each time step and to calculate the Fourier transform of all these calculated values. Then to monitor the effect for the different FDTD schemes and the use of different mesh size on the convergence of numerical eigenvalues to the exact ones.

Fig.(3.4) shows the initial condition calculated at $t = 0$ from eq.3.41 and fig.(3.5) shows the numerically calculated Fourier transform of the functional $f(t)$ as given in eq. 3.44.

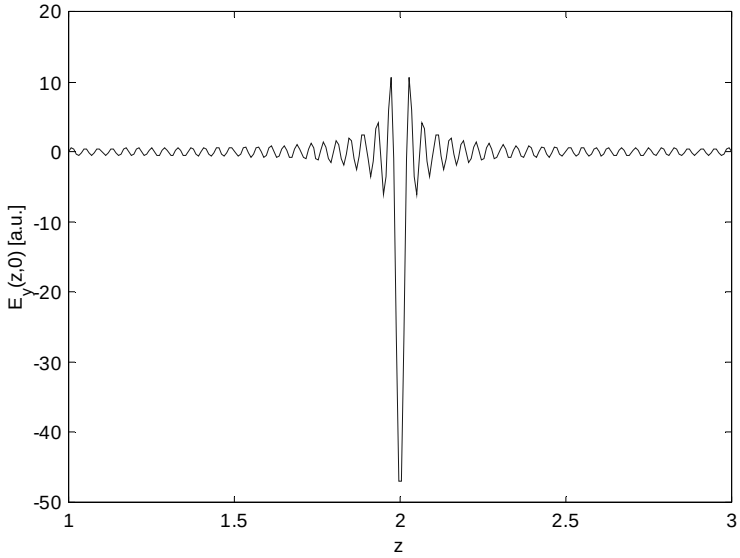

Fig.(3.4) The initial condition E(z,0) for the eigenvalue problem for assessing the dispersion of the FDTD schemes

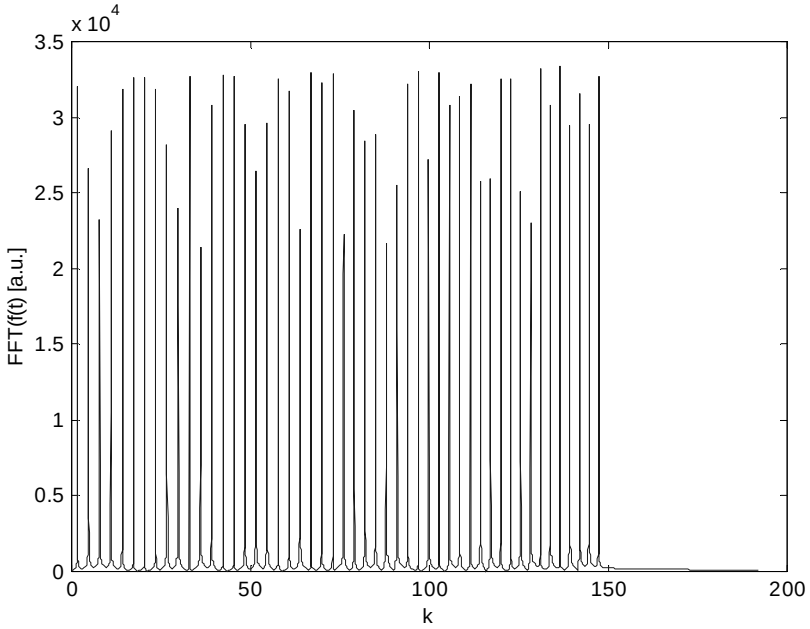

Fig.(3.5) Fourier transform for the dispersion problem. The eigenvalues are located at the positions of the peaks and the data was calculated using the Explicit(2,4) scheme.

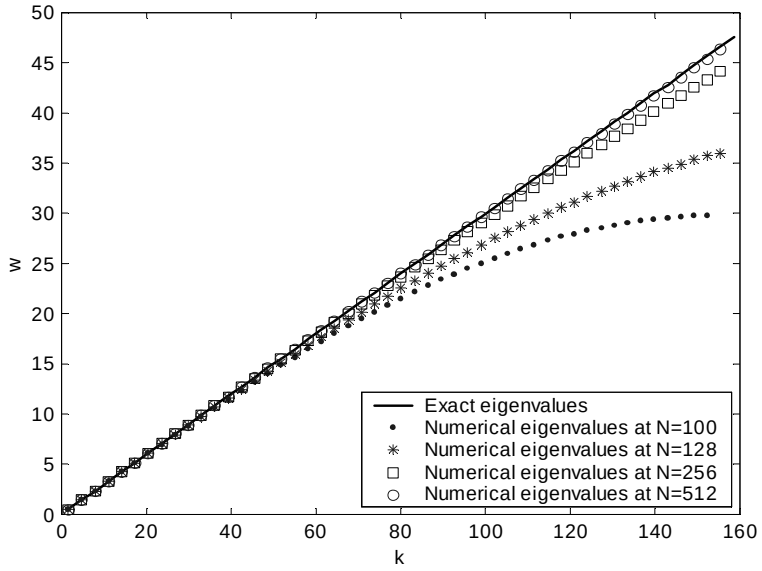

Fig.(3.6) The exact and numeric values of the wavenumbers calculated using the Yee(2,2) scheme at different mesh sizes.

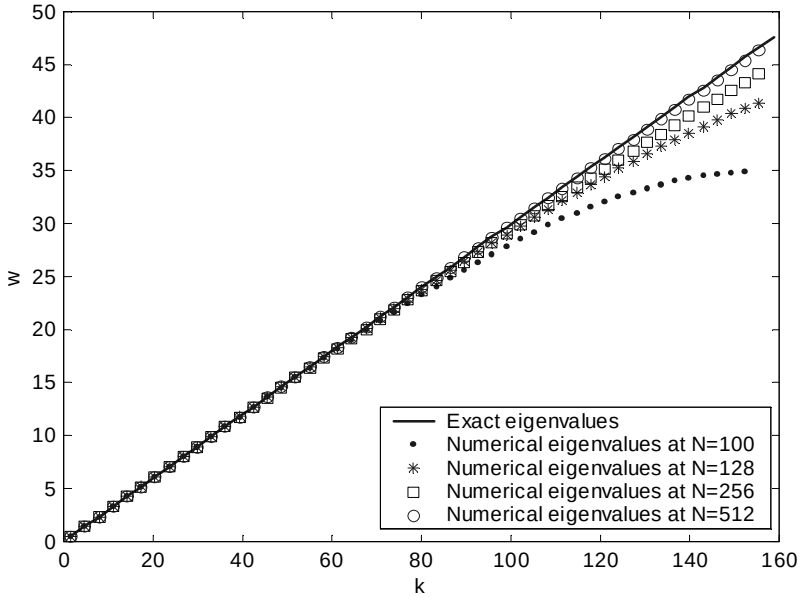

Fig.(3.7) The exact and numeric values of the wavenumbers calculated using the Explicit(2,4) scheme at different mesh sizes.

The results of the model problem are shown in fig.(3.6) and (3.7), these results were obtained for a coarse time step, which assures the improvement in the solution using the Explicit(2,4) scheme.

3.7 Conclusion

Three different FDTD scheme were presented including preliminary comparison among these schemes. Apart from the possibility of choosing arbitrary time steps when using the Implicit(2,4) scheme, the Explicit(2,4) scheme is a better choice especially when simulating large structures. The fourth order of accuracy was not achieved when simulating structures either for low or high index contrast but improvement has been observed in the results compared to those obtained by the Yee(2,2) scheme.

Chapter 4

Absorbing Boundary Conditions: The Perfectly Matched Layers

Two versions of PML are analyzed in this chapter, Berenger PML and unsplit PML [?].

4.1 How Does the PML Work?

We show explicitly in this section how the PML works. This is explained in 1D and we describe how it can be extended to higher dimensions.

As illustrated by fig.(4.1), we consider a perpendicularly incident wave from medium A, characterized by ϵ_1, μ_1, and $\eta_1 = \sqrt{\frac{\mu_1}{\epsilon_1}}$, into medium B, characterized by ϵ_2, μ_2, and $\eta_2 = \sqrt{\frac{\mu_2}{\epsilon_2}}$. The incident, reflected, and transmitted electric field component at $x = 0$ can be written in the form

$$E_k(z) = E_k^0 e^{-j\beta_k z} \tag{4.1}$$

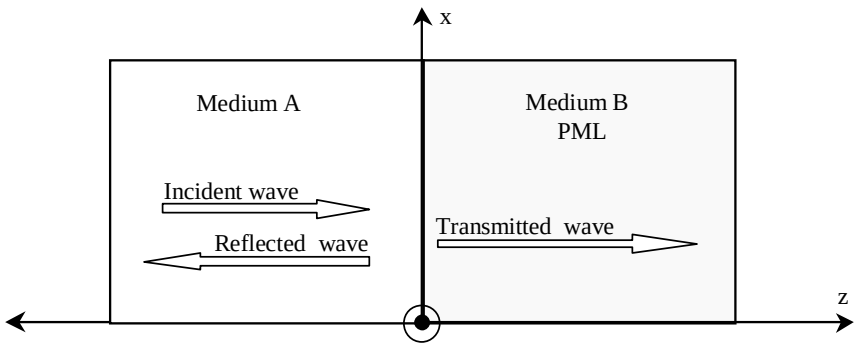

Fig.(4.1) An incident wave on a PML layer

where E_k^0 is the amplitude, β_k is the propagation constant, and $\{k = i$ for incident wave$\}$, $\{k = r$ and $\beta_r = -\beta_i$ for reflected wave$\}$, and $\{k = t$ for transmitted wave$\}$. β is written in the form

$$\beta_i = \omega\sqrt{\epsilon_i \mu_i} \tag{4.2}$$

where the index i refers to either medium A or B and ω is the angular frequency of the incident wave.

If medium A is non-dispersive, ϵ and μ of that medium are frequency independent, and if medium B is a dispersive medium characterized by an electric conductivity σ and a magnetic loss σ^*, then we have [?]

$$\epsilon_2 = \epsilon_2 \left(1 - \frac{\sigma}{j\omega\epsilon_2}\right), \tag{4.3}$$

$$\mu_2 = \mu_2 \left(1 - \frac{\sigma^*}{j\omega\mu_2}\right). \tag{4.4}$$

The reflection coefficient (the ratio of the reflected wave to the incident wave) can be calculated using the following expression

$$\Gamma = \frac{\eta_2 - \eta_1}{\eta_2 + \eta_1}. \tag{4.5}$$

If we assume that

$$\begin{aligned} \epsilon_2 &= \epsilon_1 = \epsilon \\ \mu_2 &= \mu_1 = \mu, \end{aligned} \tag{4.6}$$

and substitute equations 4.4, 4.3 in 4.5 then

$$\Gamma = \frac{\left(1 - \frac{\sigma^*}{j\omega\mu}\right)^{1/2} \left(1 - \frac{\sigma}{j\omega\epsilon}\right)^{-1/2} - 1}{\left(1 - \frac{\sigma^*}{j\omega\mu}\right)^{1/2} \left(1 - \frac{\sigma}{j\omega\epsilon}\right)^{-1/2} + 1} \tag{4.7}$$

The desired situation if medium B represents a PML medium is to have full absorption to the incident wave, $\Gamma = 0$.

Then, equating the right hand side of 4.7 to zero, the question is how to choose σ and σ^* such that $\Gamma = 0$ remains zero. A simple algebraic manipulation to eq.4.7 yields the following condition for the choice of σ and σ^*

$$\frac{\sigma}{\epsilon} = \frac{\sigma^*}{\mu}. \tag{4.8}$$

This condition is the only requirement to effectively absorb an incident wave on the PML medium.

In two dimensions, Berenger showed that splitting one of the field components into two seperate parts is an additional requirement to have zero reflection provided that eq. 4.8 is satisfied. The derivation of the PML equations have been shown in details in many references[?], [?].

4.2 Two Dimensional Berenger PML

We extend the normalization of Maxwell equations to the situation when using Berenger PML. This formulation can be easily applied to structures with homogeneous and inhomogeneous media. The extension is based on normalizing the conductivity profile that is added by the PML formulation. Following the normalization, we profile the conductivity in the PML region in such a way that we satisfy the impedance matching between the two media, the PML and the FDTD domain. This will be explained in detail, following the normalization.

We give an optimized formulation for the **2D-**TE normalized Maxwell equation, with splitting the E_y field component into two components E_{yz} and E_{yx}. Introducing the conductivity and magnetic loss terms into the non-normalized Maxwell equations, using the impedance matching condition given in 4.8, following the normalization steps explained in chapter two, we have

$$\partial_t E_{yx} = -\frac{c_0}{\epsilon_r}\partial_x H_z - \frac{\sigma_x}{\epsilon_0 \epsilon_r} E_{yx}, \tag{4.9}$$

$$\partial_t E_{yz} = \frac{c_0}{\epsilon_r}\partial_z H_x - \frac{\sigma_z}{\epsilon_0\epsilon_r}E_{yz}, \tag{4.10}$$

$$\partial_t H_x = c_0\partial_z(E_{yx} + E_{yz}) - \frac{\sigma_z}{\epsilon_0\epsilon_r}H_x, \tag{4.11}$$

$$\partial_t H_z = -c_0\partial_x(E_{yx} + E_{yz}) - \frac{\sigma_x}{\epsilon_0\epsilon_r}H_z. \tag{4.12}$$

When discretizing the previous equation, the value of either σ, σ_x or σ_z, will be zero at the inner interface of the PML region and increases gradually till **maximum value** at the outer interface.

For a PML of thickness δ and angle θ of incidence of a wave that impinges on the PML interface, the σ profile is written in the form

$$\sigma(z) = \sigma_{\max}\zeta(z). \tag{4.13}$$

The choice of $\sigma_{z\,\max}$ and $\zeta(z)$ has a great impact on the performance of the ABCs. Polynomial and geometrical grading are most commonly used for profiling the conductivity. In all our simulations in this thesis, we used the discrete polynomial grading as proposed by Berenger[**?**]

$$\zeta(z) = \left(\frac{z}{\delta}\right)^n, \tag{4.14}$$

where the boundary between the PML region an the inner domain is located at $z = 0$, with the PML extending along the positive z-axis.

More accurately the PML-shape was determined at the discretization points through integration of $\zeta(z)$ around a space cell to get the average value

$$\zeta(z_i) = \int_{z_i - \frac{\Delta_z}{2}}^{z_i + \frac{\Delta_z}{2}} \zeta(s)ds. \tag{4.15}$$

For both cases $\sigma_{z\,\max}$ was of the form

$$\sigma_{\max} = -\frac{\epsilon_0\epsilon_r c_0(n+1)\ln(R(\theta))}{2\delta\cos(\theta)}, \tag{4.16}$$

where $R(\theta)$ is the desired value of the reflectivity for the value of the incident angle θ.

Dividing $\sigma_{\max}$ by $\epsilon_0\epsilon_r$, the normalized **2D**-TE Maxwell equations with the normalized Berenger PML are

$$\partial_t E_{yx} = -\frac{c_0}{\epsilon_r}\partial_x H_z - \sigma_x E_{yx}, \tag{4.17}$$

$$\partial_t E_{yz} = \frac{c_0}{\epsilon_r}\partial_z H_x - \sigma_z E_{yz}, \tag{4.18}$$

$$\partial_t H_x = c_0\partial_z(E_{yx} + E_{yz}) - \sigma_z H_x, \tag{4.19}$$

$$\partial_t H_z = -c_0\partial_x(E_{yx} + E_{yz}) - \sigma_x H_z, \tag{4.20}$$

and the **2D**-TM Maxwell equations with the normalized Berenger PML are

$$\partial_t H_{yx} = c_0\partial_x E_z - \sigma_x H_{yx}, \tag{4.21}$$

$$\partial_t H_{yz} = -c_0\partial_z E_x - \sigma_z H_{yz}, \tag{4.22}$$

$$\partial_t E_x = -\frac{c_0}{\epsilon_r}\partial_z(H_{yx} + H_{yz}) - \sigma_z E_x, \tag{4.23}$$

$$\partial_t E_z = -\frac{c_0}{\epsilon_r}\partial_x(H_{yx} + H_{yz}) - \sigma_x E_z, \tag{4.24}$$

Fig. (4.2) shows the positions of the discretization points of the TE and TM field in the spatial **2D** Yee FDTD grid.

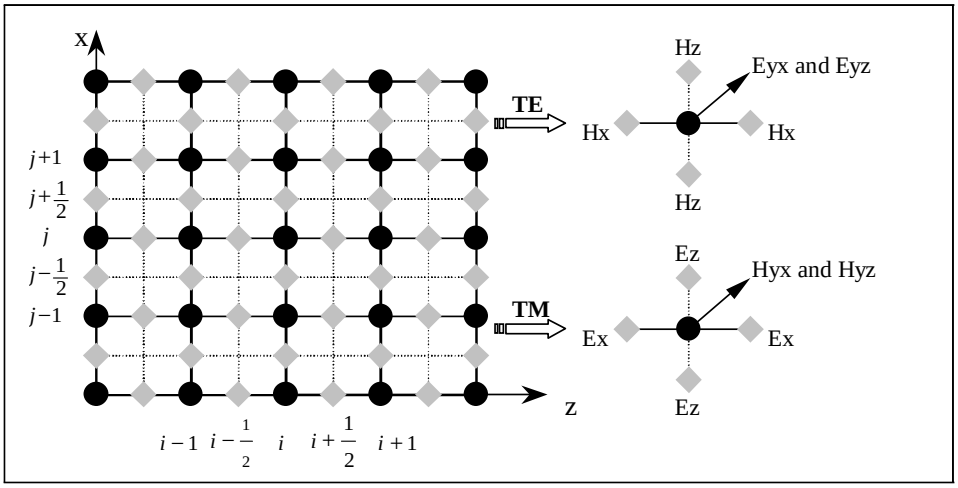

Fig.(4.2) A 2D staggered lattice structure, The Yee lattice

Another advantage when using this normalization that was briefly mentioned in chapter two is the fact that working with small or large constants is totally avoided since niether the value of ϵ_0 nor μ_0 is explicity used in addition, always when discretizing these equations the time step, which is in femto seconds, will be multiplied by the speed of light, c_0.

In the next section we derive the normalized unsplit PML formulation and show that its approximation is equivalent to the Berenger PML formulation.

4.3 Two Dimensional Unsplit PML Formulation

When numerically discretizing the Maxwell's equations and depending on the problem and materials that are being modeled, the use of unsplit PML will be shown to be more efficient than using the conventional Berenger PML. The unsplit PML [?], [?] is well suited for modeling dispersive materials either in frequency or time domain. Although throughout this work we only considered non-dispersive media, still one can use the unsplit PML formulation. We derive the normalized unsplit PML TE and TM fields and show that they are approximately equaivalent to the Berenger PML TE and TM fields.

For reasons that will become clear later in this section, the set of three equations $\partial_t \mathbf{D} = c_0 \nabla \times \mathbf{H}$, $\mathbf{D}(\boldsymbol{\omega}) = \epsilon_r(\omega)\mathbf{E}(\boldsymbol{\omega})$, and $\partial_t \mathbf{H} = -c_0 \nabla \times \mathbf{E}$, where $\mathbf{D}$ is used a third field variable, will be used alternatively, we name this the **DEH** set.

The TE fields for the **DEH** set will have the form

$$j\omega D_y = -c_0(\partial_x H_z - \partial_z H_x), \tag{4.25}$$

$$E_y(\omega) = \epsilon_r(\omega) D_y(\omega), \tag{4.26}$$

$$j\omega H_x = c_0 \partial_z E_y, \tag{4.27}$$

$$j\omega H_z = -c_0 \partial_x E_y, \tag{4.28}$$

and the TM fields will have the form

$$j\omega H_y = c_0(\partial_x E_z - \partial_z E_x), \tag{4.29}$$

$$j\omega D_x = -c_0 \partial_z H_y, \tag{4.30}$$

$$E_x(\omega) = \epsilon_r(\omega) D_x(\omega), \tag{4.31}$$

$$j\omega D_z = c_0 \partial_x H_y, \tag{4.32}$$

$$E_z(\omega) = \epsilon_r(\omega) D_z(\omega), \tag{4.33}$$

Equations 4.25-4.33 are in the frequency domain and have to be transformed to the time domain, $j\omega$ in frequency domain becomes $\frac{d}{dt}$ in the time domain and $\frac{1}{j\omega}$ becomes $\int$.

The TE fields with unsplit PML is written in the form [?]

$$j\omega \left(1 + \frac{\sigma_x}{j\omega}\right)\left(1 + \frac{\sigma_z}{j\omega}\right) D_y = -c_0(\partial_x H_z - \partial_z H_x), \tag{4.34}$$

$$E_y(\omega) = \epsilon_r(\omega) D_y(\omega), \tag{4.35}$$

$$j\omega \left(1 + \frac{\sigma_x}{j\omega}\right)^{-1}\left(1 + \frac{\sigma_z}{j\omega}\right) H_x = c_0 \partial_z E_y, \tag{4.36}$$

$$j\omega \left(1 + \frac{\sigma_x}{j\omega}\right)\left(1 + \frac{\sigma_z}{j\omega}\right)^{-1} H_z = -c_0 \partial_x E_y, \tag{4.37}$$

and for the TM fields

$$j\omega \left(1 + \frac{\sigma_x}{j\omega}\right)\left(1 + \frac{\sigma_z}{j\omega}\right) H_y = c_0(\partial_x E_z - \partial_z E_x), \tag{4.38}$$

$$j\omega \left(1 + \frac{\sigma_x}{j\omega}\right)^{-1}\left(1 + \frac{\sigma_z}{j\omega}\right) D_x = -c_0 \partial_z H_y, \tag{4.39}$$

$$E_x(\omega) = \epsilon_r(\omega) D_x(\omega), \tag{4.40}$$

$$j\omega \left(1 + \frac{\sigma_x}{j\omega}\right)\left(1 + \frac{\sigma_z}{j\omega}\right)^{-1} D_z = c_0 \partial_x H_y, \tag{4.41}$$

$$E_z(\omega) = \epsilon_r(\omega) D_z(\omega). \tag{4.42}$$

If we move every thing to time domain in eq.4.34-4.37, substitute 4.35 in 4.34, splitting E_y into $E_{yx} + E_{yz}$, and finally neglect the term $\sigma_z \sigma_x$ we get the equivalent equation in the Berenger PML formulation.

Getting the time domain discretization of the unsplit PML formulation is not a straight forward approach and requires introducing new variables that are non-zero only in the PML layers. We describe the main lines to get such discretization, details can be found in [?].

We consider the TM fields given in eq. 4.38-4.39. Moving every thing to time domain in eq.4.38, eq. 4.39 and eq.4.41 will be treated in similar to eq.4.38,

$$\partial_t H_y + \sigma_x H_y + \sigma_z H_y + \sigma_z \sigma_x \int_0^t H_y(s) ds = c_0(\partial_x E_z - \partial_z E_x), \tag{4.43}$$

with the following discrete form for the left hand side of eq.4.43

$$\frac{H_y|_{i,j}^{n+1} - H_y|_{i,j}^{n}}{\triangle t} + \left(\sigma_z|_i + \sigma_x|_j\right) \frac{H_y|_{i,j}^{n+1} + H_y|_{i,j}^{n}}{2} + \sigma_z|_i \, \sigma_x|_j \sum_{s=0}^{n} \left(H_y|_{i,j}^{s+1} + H_y|_{i,j}^{s}\right) \tag{4.44}$$

It is clear that in addition to the extra field variables, D_x and D_z in TM fields and the additional operations to update the basic fields, E_x and E_z, extra variables need to be defined in the PML regions at all time steps to store the accumulated sums of field values. However, due to the fact that the values both σ_z and σ_x range from 0 to 1, a possible approximation could be to neglect the term $\sigma_z \sigma_x \int_0^T H_y(s) ds$ in eq.4.43.

A preliminary comparison between the two formulation leads to the following

- Unsplit PML present a direct and simple treatment to dispersive or nonlinear media. This is because all the characteristics of the media are preserved in eq. 4.26, TE fields.
- Unsplit PML introduces new field components and additional components that needed to be calculated and stored for all time steps. Nevertheless, some of these additional variables are non-zero in the PML regions only. In addition to the storage requirements for the additional variables, the computational time increases per time iteration.

The implementation of unsplit PML formulation for waveguide problems or dispersive materials was not consider in this work and was left for future work.

4.4 Choice of the PML Parameters

The performance of PML-ABCs is controlled by choosing carefully its parameters. These are the number of PML cells, the width, the polynomial degree of the conductivity profile, and finally the desired value for the reflectivity. To choose these parameters we consider a **1D** problem in which two different simulations are performed simultaneously. The first one is the test simulation and the second one is the reference simulation. A sinusoidal wave with wavelength 1.0 μm is excited as a hard source, details are in chapter five, and is allowed to propagate 5 μm in the z-direction. On the right boundary of the inner region the **1D** region a PML with different values for its parameters is implemented. The time step and the number of iterations were chosen so as to ensure that the wave propagating in the reference problem will not encounter any effect from the BCs; i.e. the reference problem runs on extended computational domain. Then, using the reference and test simulation the global error is calculated, which is squared difference between the solutions in the two simulations. This is then added to accumlate the overall global error of the entire simulation. Fig.(4.3)-fig(4.6) show the variation of this error as a function of the PML parameters. When looking for the best values for one of the PML parameters the others were chosen optimally. From these figures we see that 12 cells for the PML width, quadratic polynomial degree, and a reflectivity of value 10 are a good choice for the PML parameters.

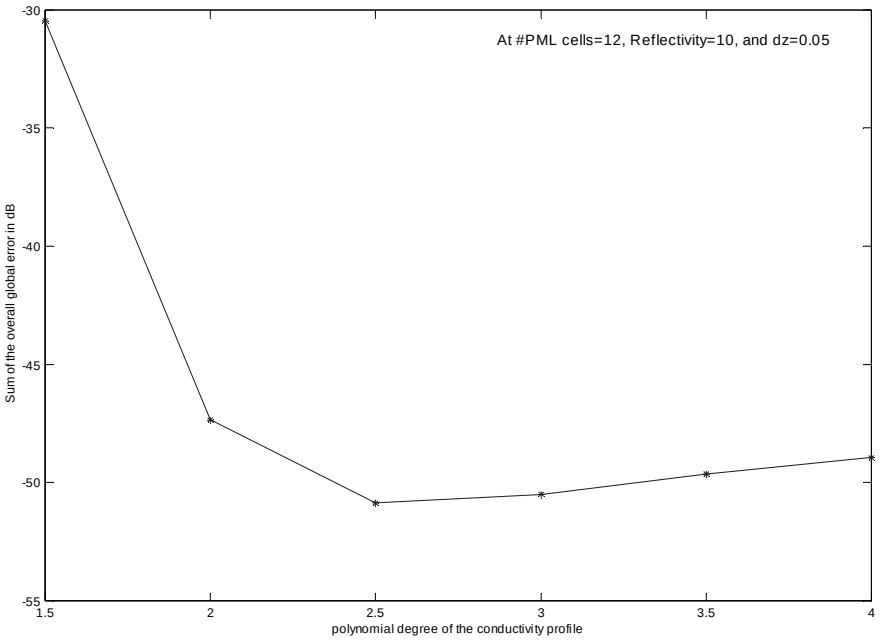

Fig.(4.3) Overall global error as a function of the polynomial degree of the conductivity

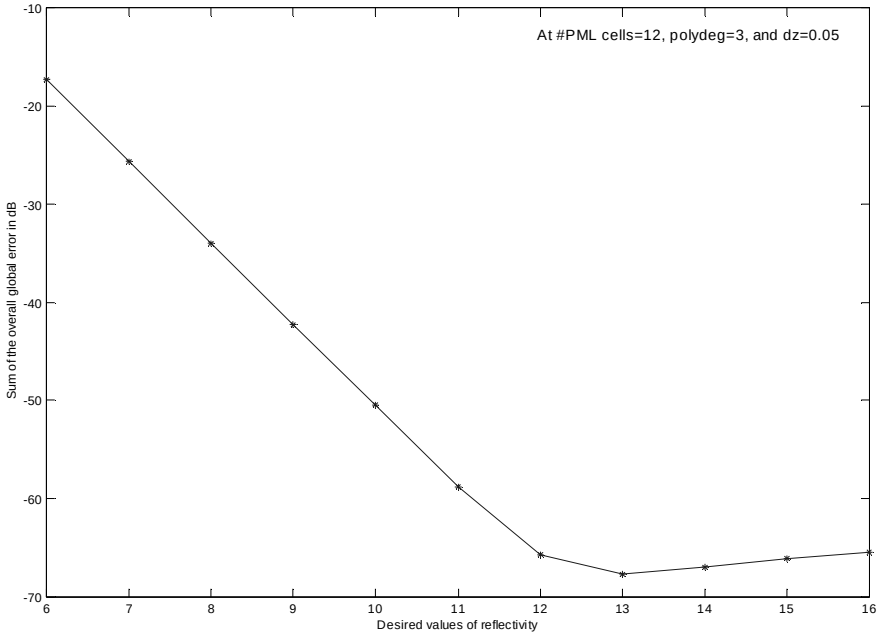

Fig.(4.4) Overall global error as a function of the desired reflectivity

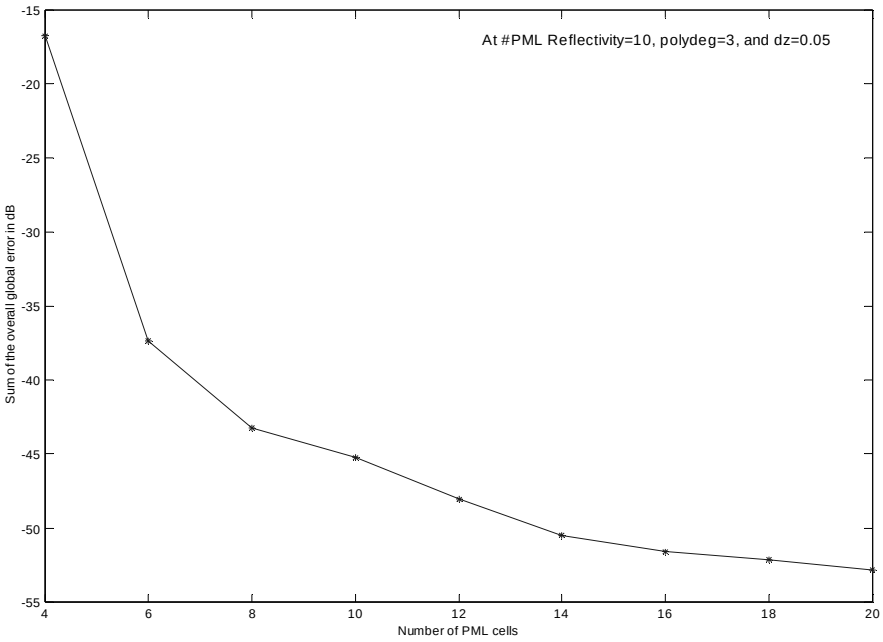

Fig.(4.5) Overall global error as a function of the number of PML cells

4.5 Numerical and Implementation Concerns for the PML and Unsplit PML Formulations

In this section we discuss possible ways to implement the discretized Maxwell equations with either the Berenger PML or the unsplit PML. In addition, we show how to profile the PML conductivity such that extended waveguides beyond the computational window can be simulated. Finally, we analyze and select the most efficient and minimized cost implementation.

Fig(4.6) shows the computational domain that is divided into two regions, the FDTD main region and the PML region. The PML region is divided into eight subregions, front PML, back PML, left PML, right PML, and four corners. If a waveguide is to be simulated and in order to allow transimitted fields or back reflected fields to be absorbed totally in the PML regions, the waveguide is extended into the PML regions as shown in fig(4.6). In the same time the matrix of the dielectric constant ϵ_r is expanded to cover the PML regions. The crucial point is that the expansion of this matrix should guarantee that two neighboring points in the PML and FDTD domain have the same value in order to satisfy the impedance match condition to avoid any back reflection, see the first section of this chapter.

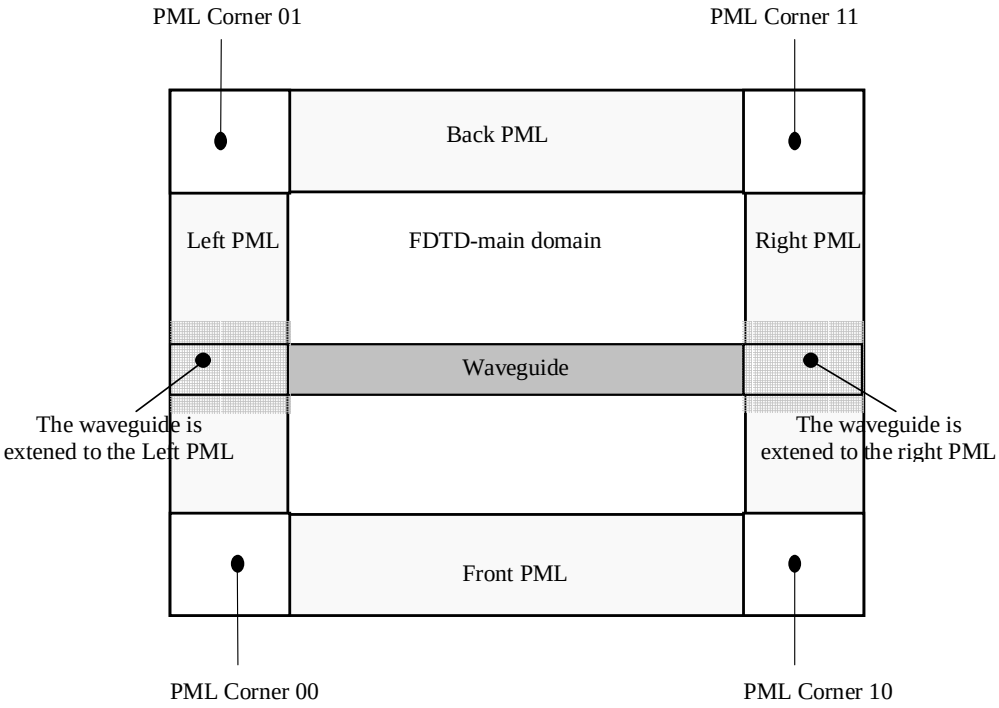

Fig.(4.6) A simulated waveguide extended into the PML regions in **2D**.

The conductivity values for σ_z, similarly for σ_x, in the PML regions do not require to have any information about the material properties of the PML regions. The main advantages is that σ_z will be filled in a line in the z- direction. The values of σ_z along this line will be the same alone the x-direction.

For the original split-field PML technique, there are two possible ways to discretize the field components in the PML and inner domain domain regions. The first is to define all the fields components including the splitted fields for the two domains. The other possibility is to work with the split-field formulation in the PML regions and to work within the inner region with the normalized Maxwell equations at zero conductivity. Both approaches have advantages and disadvantages and the choice depends on the size of the problem. When choosing the second approach, one has to keep track of the intersections between the PML and inner domain where E_y is the sum of E_{yx} and E_{yz} in the PML regions for **TE** fields. The situation becomes even more complicated when using higher order FDTD schemes for which long stencil discretizations are employed.

4.6 Conclusion

Two versions of PML-ABCs were presented, the Berenger PML and the unsplit PML. It depends on the problem, which of these is to be used. Berenger PML is well suited and computationally efficient for modelling non-dispersive and linear materials. On the other hand, the unsplit PML can simply be applied to more complex materials as well as to simple ones. The unsplit PML introduces additional field variables and parameters and hence requires more computational time and resources.

Chapter 5

Sources in FDTD Simulation

Exactly controlling the power of the input signals that are introduced into the FDTD grid, avoiding the interaction between simulated sources and the ABCs, and decreasing the load on the ABCs are the most challenging problems in waveguide simulation problems. The situation becomes more difficult, if information about fields reflected back from any scatterer inside the problem domain is of practical interest.

There are different techniques that are commonly used for exciting waveguide structures simulated by the FDTD method. These techniques are: hard source excitation, transparent sources [**?**], and total-field/scattered-field(TF/SF) formulation [**?**].

All of these techniques aim at assigning the input field to one or more field components and in the same time allow any reflected wave to pass through the input field.

We briefly introduce and compare the effectiveness, applicability, and ease of implementation of these techniques.

5.1 Hard Source Excitation

Hard source excitation is the simplest way to excite fields in FDTD simulations. The hard source excitation is implemented by specifying one or more field components at a given grid point, line, or plane with a temporal driven function. The major drawback from using the hard source excitation is that a hard source disregards any wave that is reflected back to the excitation position and therefore it acts as a perfect reflector. Despite this severe disadvantage, hard source excitation was used in our work in different situations.

The first occasion of hard source excitation was when assessing the accuracy of the different high order FDTD schemes applied in **1D** TE discussed in chapter four. Only the E_y field was assigned through a driving function at the left grid point of the grid, only PMLs-ABCs were used at the right side of the domain. The second use of hard source excitation was as a part of implementing the TF/SF formulation; details will be explained in the TF/SF section. The third occasion with hard source excitation was to introduce the incident fields by propagating them through PML regions [**?**]. We will explain this in details in the following section.

5.2 Excitation Through PMLs Window

The incident field is introduced as a hard source, mathematically speaking, as Dirichlet BC, at the left grid point or line of the grid and is then propagated through the PMLs. The attenuation effect of the PMLs is taken into account and used to scale the input field such that fields that reach the inner side of the left PML will have the same values as if the original one would be present.

In order to couple the exact power to the inner lattice one has to run a simulation till the wave reaches the inner boundary of the PMLs and calculate the amplification factor for the hard souce outside the PML region. Fortunately, the first simulation need neither to run till the last time step nor for the same grid size as the original one. Only a time and grid size is required that is sufficient enough to accurately determine the correct amplification factor.

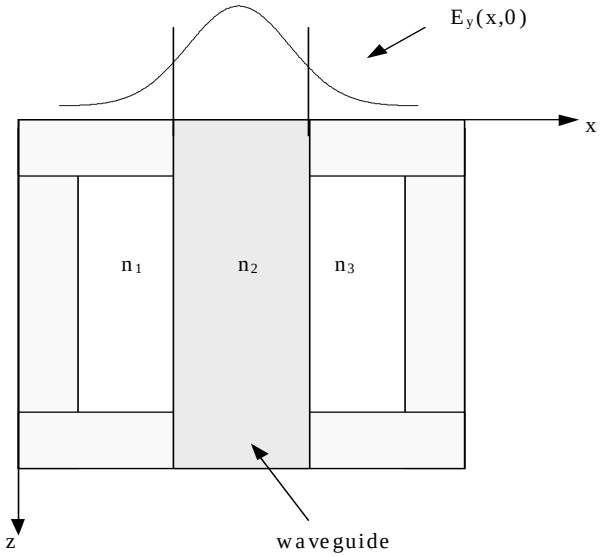

Fig.(5.1) introducing incident fields through the PML region

The attenuation of PMLs with width δ in the z-direction is calculated as

$$A = e^{-kn \int_0^{\delta} \sigma_z(z) dz}, \tag{5.1}$$

where $\sigma_z(z)$ is the profile of the conductivity given in the PML region, n is the refractive index, which for guided modes is replaced by the effective index, and k is the wavenumber. For a structure as shown in fig.(5.1), the mode profile is multiplied by the amplification factor that is initially $1/A$ and which is corrected for the first run of the desired simulation.

This excitation procedure was implemented in **1D**. A sinusoidal wave with wavelength 1.25 μm is introduced at the outer edge of the PML domain and is propagated inside the PML. The length of the **1D** domain is 5 μm and the spatial step size was 0.025 μm. The PML parameters are selected similar to those chosen in previous simulations, the time step was 0.02 fs, and the wave is propagated a period of 100 fs. The amplification factor is calculated according to eq. 5.1. Fig.(5.2) shows, in the upper figure, the plot of the E_y field as calculated with the Yee(2,2) scheme. In the lower figure the correct amplification factor was applied and the desired power was excited into the inner domain. Using the same configurations of the **1D** problem, the same amplification factor and excitation procedure, the figure shows that the Explicit(2,4) does not lead to the desired result. It is clear from this example that the performance of the PML is scheme dependent. The extension of this formulation to **2D** waveguide problems was not investigated and was left for future work.

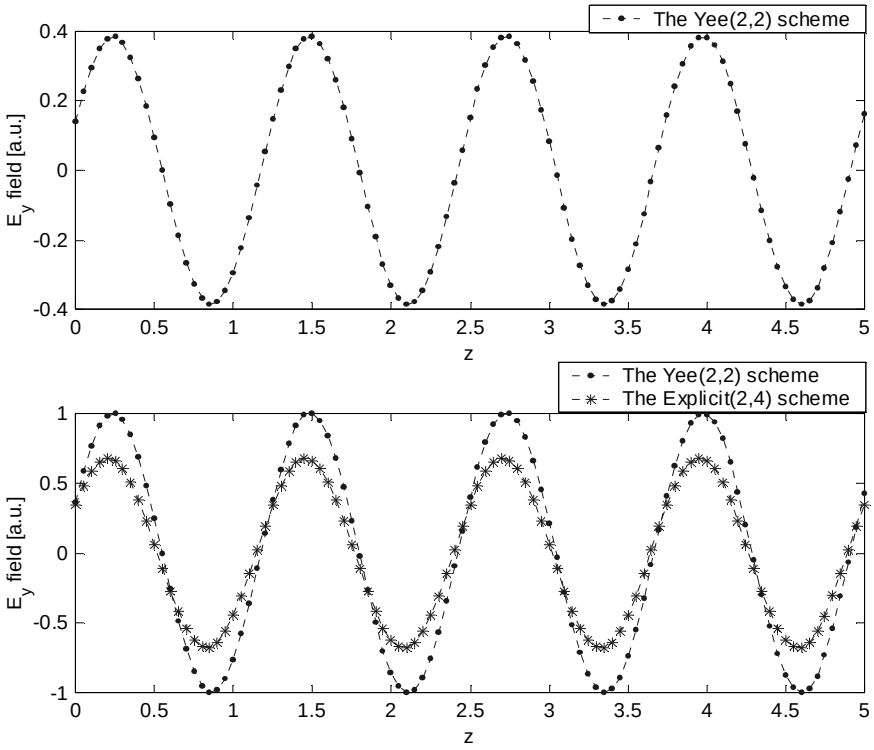

Fig.(5.2) Excitation of **1D** FDTD through left PML region for use with the Yee(2,2) scheme and the Explicit(2,4) scheme.

A drawback from this excitation technique is that the load on the PMLs will be higher especially in the presence of any scatterer that is positioned perpendicular to the direction of the incident source. In that case and due to the reflection characteristics of the hard source excitation described before, it is no longer guaranteed that the same power will be introduced to the FDTD grid!. In addition it is not possible any more to get any information about any scattered field.

5.3 Transparent Source Excitation

The transparent source excitation [**?**], [**?**] is based on introducing the incident field at the inner PML-FDTD domain interface by propagating two waves, the desired one and another one to be absorbed in the PML domain. The implementation is done by setting the value of one of the field components at a source point, in case of a **1D** grid for example, equal to the sum of the field calculated from the FDTD update equations and the incident field. Any field that is reflected back to the source point will pass through it and in this sense the source point is "transparent".

This simple transparent excitation technique does not couple the same power to the FDTD grid as a hard source does. To avoid that, additional storage and calculation time is required. The difference between the power introduced by the transparent excitation and the desired power is caused by what is called grid impulse response. Hence, storing and subtracting this grid impulse response at the excitation positions is the main idea of transparent excitation.

We show how to implement transparent source excitation in **1D** and how it can be extended to **2D**. Considering the discretized **1D** TE fields given in eq. 3.12 and eq.3.13, a first transparent excitation will be, for $\epsilon_r = 1$,

$$E_y|_i^{n+1} = E_y|_i^n + \frac{c_0 \triangle t}{\triangle z}\left(H_x|_i^{n+\frac{1}{2}} - H_x|_{i-1}^{n+\frac{1}{2}}\right), \quad i \neq p \tag{5.2}$$

$$E_y|_i^{n+1} = E_y|_i^n + \frac{c_0 \triangle t}{\triangle z}\left(H_x|_i^{n+\frac{1}{2}} - H_x|_{i-1}^{n+\frac{1}{2}}\right) + f_i^{n+1}, \quad i = p \tag{5.3}$$

$$H_x|_{i+\frac{1}{2}}^{n+\frac{1}{2}} = H_x|_{i+\frac{1}{2}}^{n-\frac{1}{2}} + \frac{c_0 \triangle t}{\triangle z}\left(E_y|_{i+1}^n - E_y|_i^n\right), \tag{5.4}$$

where f_p^{n+1} is the incident field at the incidence position with index p. Eq. 5.2-5.4 do not couple the same power to the **1D** FDTD grid. We show explicitly how to avoid that by modifying eq. 5.3 and monitoring the values of E_y at the incidence position p at the first time steps, assuming that $\frac{c_0 \triangle t}{\triangle z}$, the courant number is 1 :

$$E_y|_p^0 = f_p^0, \tag{5.5}$$

$$E_y|_p^1 = E_y|_p^0 + \left(H_x|_p^{\frac{1}{2}} - H_x|_{p-1}^{\frac{1}{2}}\right) + f_p^1 + f_p^0, \tag{5.6}$$

Calculating $H_x|_p^{\frac{1}{2}}$ and $H_x|_{p-1}^{\frac{1}{2}}$ from eq.5.4 and substituting the results in eq. 5.6 result in

$$E_y|_p^1 = f_p^1, \tag{5.7}$$

which is the desired value at the excitation positions. Extending this formulation for any courant number is not straightforward and more involved in higher dimension. In **1D** a power adjusted transparent source excitation is obtained by replacing eq.5.4 by the following equation

$$E_y|_i^{n+1} = E_y|_i^n + \frac{c_0 \triangle t}{\triangle z}\left(H_x|_i^{n+\frac{1}{2}} - H_x|_{i-1}^{n+\frac{1}{2}}\right) + f_i^{n+1} - \sum_{m=0}^{n} I_p^{n-m+1} f_p^m, \quad i = p, \tag{5.8}$$

where I_p^k is the grid impulse response at time step k and the sum term is the cancellation term that assures to have the adquate power at the excitation location. The grid impulse response is obtained by exciting the FDTD grid by a Kronecker delta function [**?**], and by calculating the grid impulse response from the following update equation

$$I_i^n = E_i^{n-1} + \frac{c_0 \triangle t}{\triangle z}\left(H_x|_i^{n-\frac{1}{2}} - H_x|_{i-1}^{n-\frac{1}{2}}\right), \quad i = p \tag{5.9}$$

The same procedure is extendable to higher dimensions and one has to run a FDTD simulation to calculate and store the grid impulse response for the same structure of interest. Due to the time limitation we only implemented this formulation in **1D** and **2D** during development of the PML-ABCs but without caring about power adjustment as explained here. Despite the time and storage requirements, in our opinion, this formulation is one the most efficient excitation techniques. Fig.(5.3) shows a plot of the E_y field component for a symmetric Y-junction that is excited by this formulation. Visually one can see that the expected physical behavior for this device is simulated even when the power was not adjusted.

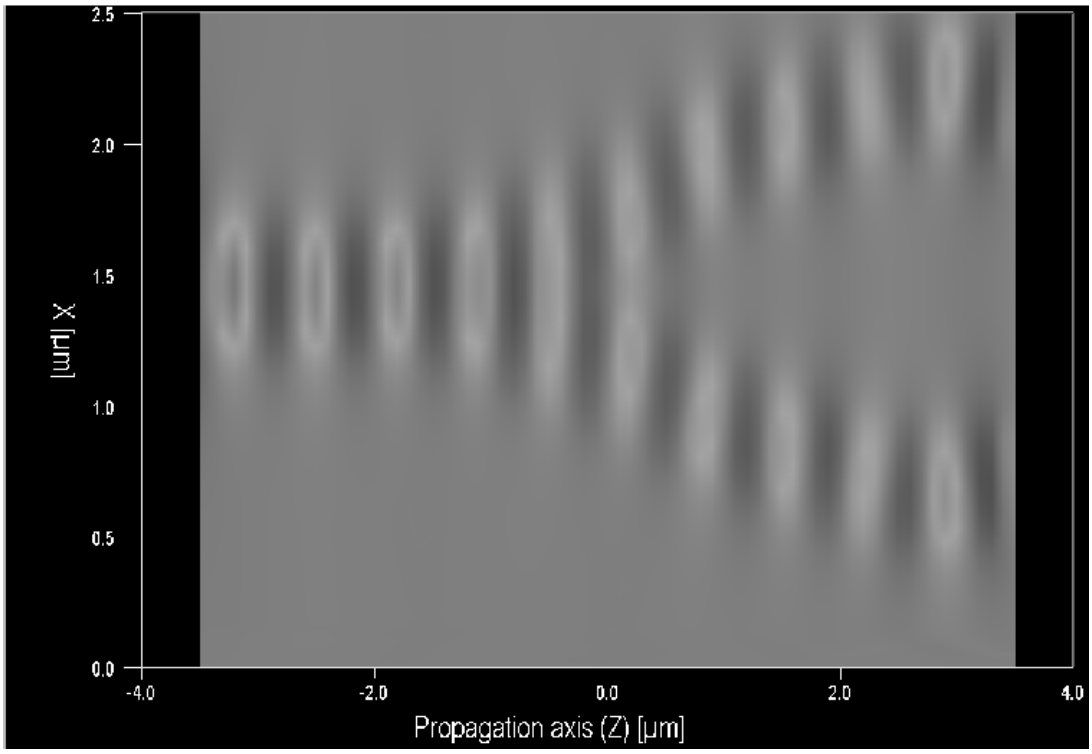

Fig.(5.3) The plot of E_y field component of a symmetric Y-junction using transparent source excitation.

5.4 One-Sided vs. Two-sided Total-Field/Scattered-Field Formulation

The total-field/scattered-field (TF/SF) technique [**?**] is an efficient way to increase the quality of simulations through reducing the load on the ABCs and by offering information about scattered fields. This comes at a high cost due to the need to run the simulations twice, or two simultaneous simulations, as will be explained in this section.

The simulation domain is divided into three domains: the total-field domain, the scattered field domain, and the PML domain, as in Fig (5.4). The formulation is based on the linearity of the Maxwell equations and on decomposing the electric and magnetic fields as sum of two components, one in the total field region and the another in the scattered field region

$$E_t = E_i + E_s, \tag{5.10}$$

$$H_t = H_i + H_s, \tag{5.11}$$

where ξ_i is the incident field value, ξ_s is the scattered field value, and ξ_t is the total field value, with $\xi = \{E, H\}$.

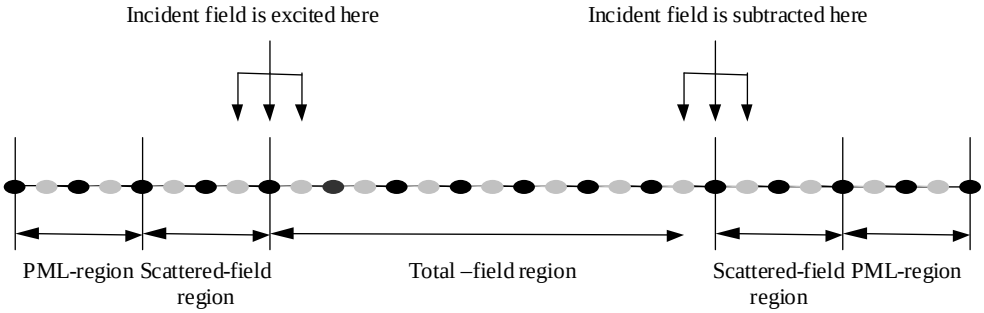

Fig. (5.4) The FDTD regions for 1D TF/SF grid.

Consider the **1D** mesh as shown in fig.(5.4). This represents a two-sided TF/SF formulation. The black dots are the positions of the electric field, E_y, and the gray dots are the positions of the magnetic field H_x. In the total-field region, the FDTD algorithm is applied to the total field, while in the scattered-field region it is applied to scattered field only. On the interface between these two regions the incident field is taken into account. Details of these formulation in **1D**, **2D**, and **3D** are well documented in [**?**].

For the **1D**-Yee(2,2) scheme, only two FDTD update equations need modification. The first for the E_y field update equation at the TF-SF interface and the second for the H_x field update equation at the first point to the left to the TF-SF interface [**?**]. The same formulation is extended to the Explicit(2,4) scheme where three E_y field update equation and two three H_x update equations are modified.

A drawback from the TF/SF formulation is that fields that are in the scattered field region do not accurately represent the physical field originating from a scatterer inside the domain. To explain this, the TF/SF formulation is implemented with the Yee(2,2) and the Explicit(2,4) schemes and a sinusoidal wave is allowed to propagate in the absence of any scatterer in the domain. Although there should be no field in the SF region, field is observed as shown in fig.(5.5). Nevertheless the intensity of the field in SF region is approximately 10^{-5} of the intensity of the field inside the TF region.

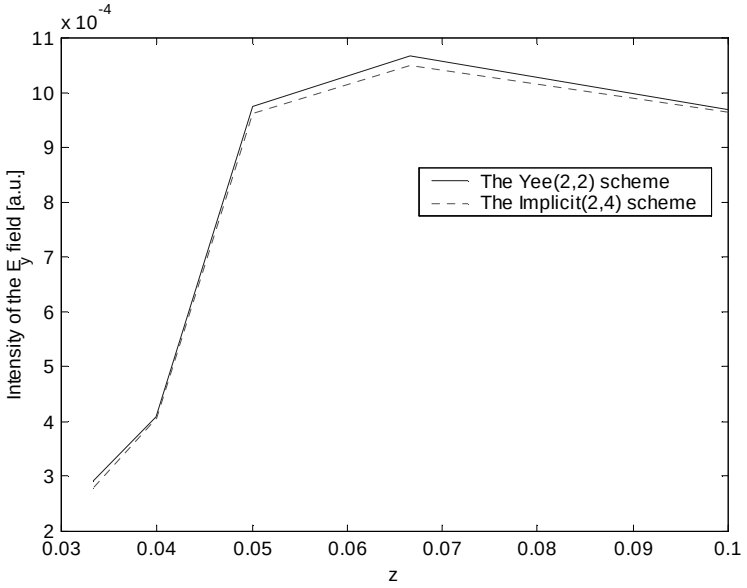

Fig.(5.5) the intensity of the E_y field in the SF region.

The TF/SF was originally proposed for free space problems and for modeling point sources which are not of great practical interest in integrated optics problems. We explain how we extended this approach to waveguide problems. Fig.(5.6) shows the division of the domain as utilized for our one-sided TF/SF.

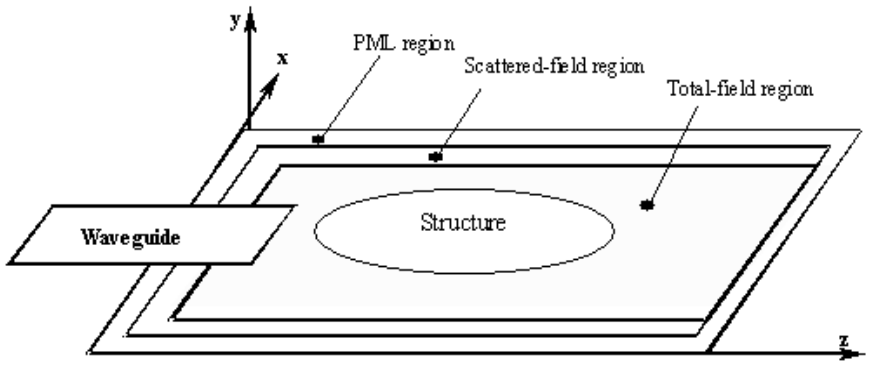

Fig.(5.6) **2D** one sided-TF/SF problem geometry.

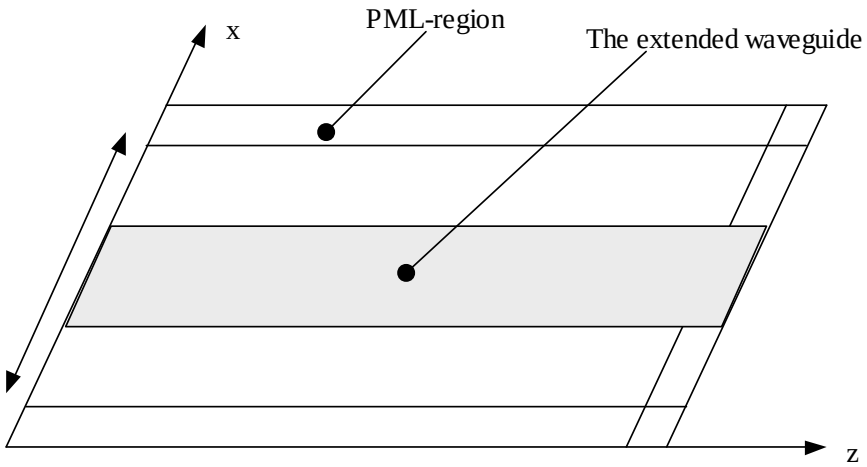

Fig.(5.7) 2D-problem domain for simulation of the incident field in the absence of any structures inside the TF region

Two different structures are simulated simultaneously. In the first simulation the waveguide that is used to excite any structure inside the TF region is extended to the right hand side of the domain, see fig.(5.7). The waveguide is then excited by the incident field using the hard source formulation such the exact power is coupled to the FDTD grid, no left PMLs-region is used. In the second simulation with the configuration shown in fig.(5.6), fields obtained from the first simulation are used to introduce the incident field. For most of our simulations the SF region was the same as the PML region. thinner PML regions may be used due to the fact that the load on the PML will be extremely lower.

Fig.(5.9) shows the intensity plot of the E_y field for TE polarization for the cos-bend waveguide sketched in fig.(5.8), with width 0.5 μm, length 10 μm, offset 2 μm, and $d\alpha$ 0.1 μm. At the plane in and plane out positions the cos-bend is connected to a waveguide with the same width of the cos-bend and a length 2 μm. The refractive index of the background is 1.0 and a refractive index of 3.0 in the guiding regions. The computational window is 5×15 μm in the x- and z-directions, and the wavelength is 1.5 μm, $\triangle z$ and $\triangle x$ were chosen to be 0.05 μm and simulation is performed

for 300 fs with dt equal to 0.05 fs: The values for the PML parameters are 8, 3, 10 for the number of PMLs cells, the polynomial degree of the conductivity profile, and the reflectivity, respectively, in both the z- and x-directions. Fig.(5.10) shows the intensity of the incident field propagating in the extended waveguide.

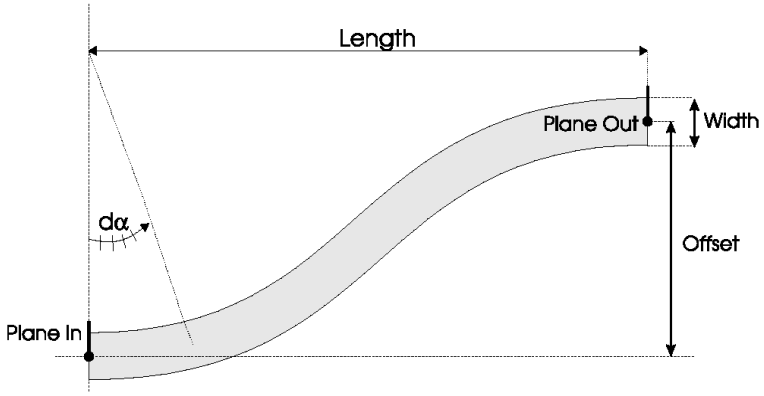

Fig.(5.8) Cos-bend

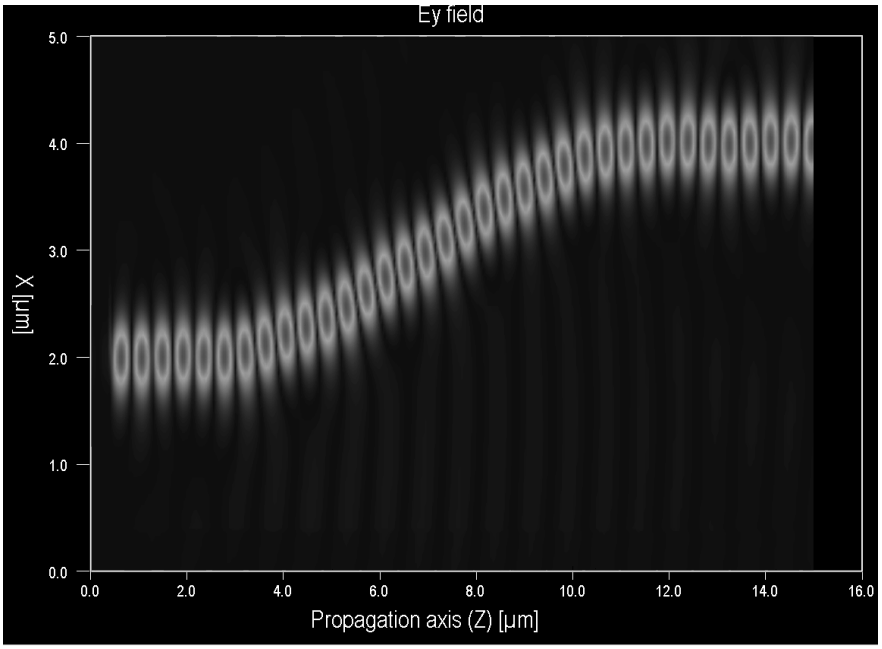

Fig.(5.9) The intensity plot of TE-E_y field propagating in a cos-bend waveguide using the TF/SF formulation.

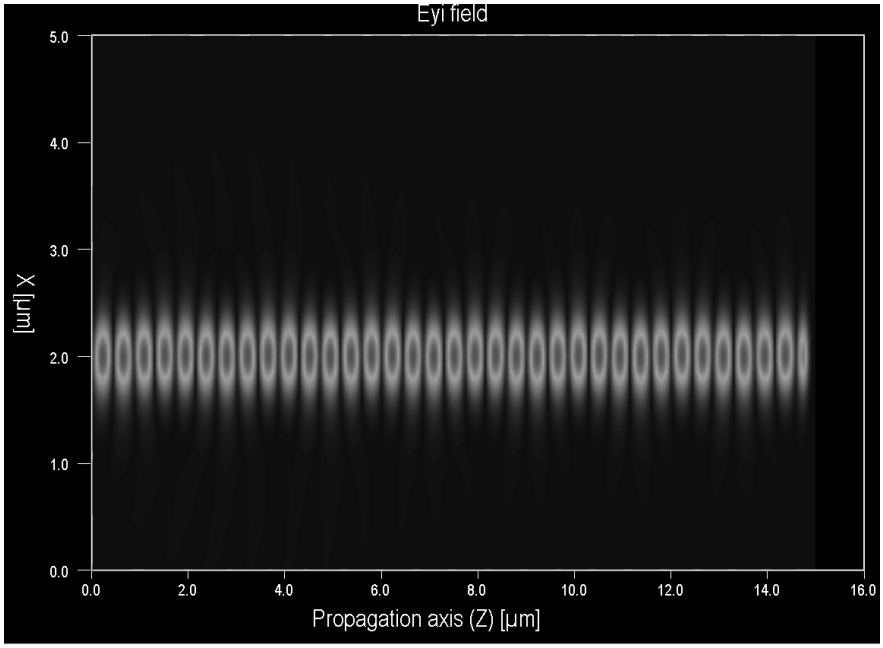

Fig.(5.10) The intensity plot of TE-E_y field propagating in an extended waveguide used in the TF/SF excitation.

Another example that approves the performance of this excitation is shown in fig.(5.11) which is the intensity plot of the E_y component resulting from excitation of a straight waveguide of width $1\mu m$ and length 4 μm. The waveguide was excited by the first order mode. The refractive indices are 1.0 for the background and 1.5 inside the waveguide. The wavelength is 1.0 μm, the computational window is 4×4 μm^2 with $\triangle z$=$\triangle x$=0.02 μm. The simulation is performed for 40 fs, dt=0.02 fs: The values of the PML paramters were chosen to be similar to those used in simulating the cos-bend, also they were standard in most of our simulations

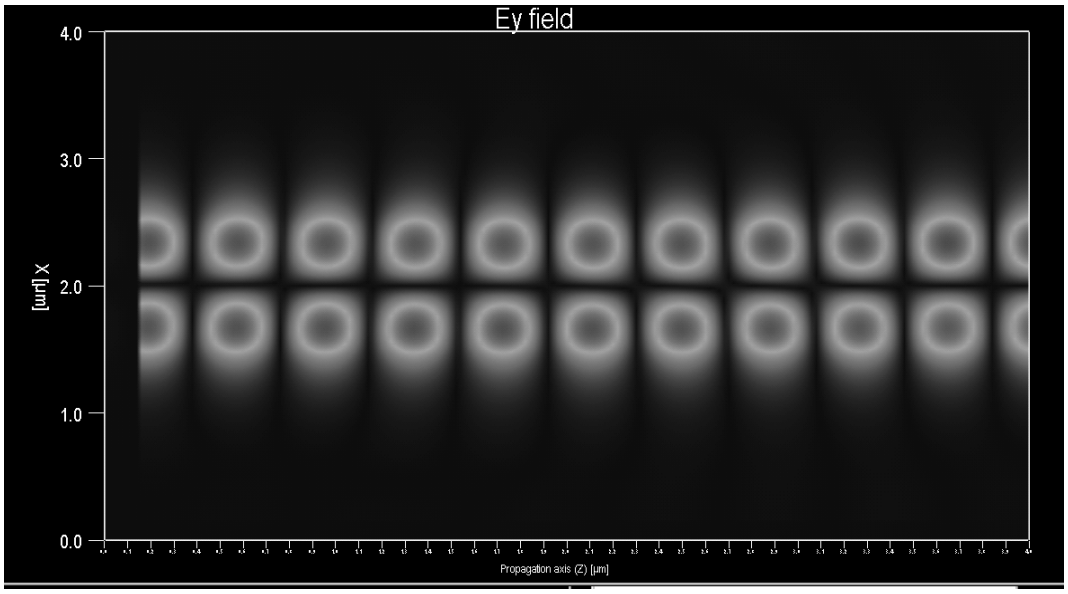

Fig.(5.11) The intensity plot of E_y field for a straight waveguide excited by the first order mode using the TF/SF formulation.

5.5 Conclusion

Different excitation techniques were investigated in **1D**. The TF/SF formulation was implemented and tested in **2D**. Our developed TF/SF excitation for waveguide problems proved to be a good excitation technique in launching the exact power as well as decreasing the load on the PML-ABCs. Still the formulation needs to be optimized especially with regard to the size of the simulation structure that is used to excite the structure of interest.

Chapter 6

Application of FDTD to 2D Integrated Optical Devices

In this chapter we employ the FDTD solver to analyze a number of **2D** structures. In order to assess the performance of the solver and the accuracy of the results, a number of post-processing tools need to be implemented such as overlap calculations. Implementing such functions is not that much work at all but implementing them in the environment of Prometheus program in which we implemented our FDTD tools require more time which was not available at the end of this work. Therefore part of our assessment will depend on the physical behavior of devices under testing, visual assessment. It is clear from the results presented in the previous and current chapter that the performance of our tools is extremely good especially with regard to the ABCs and our developed excitation procedure.

6.1 Waveguides

Fig.(6.1) and fig(6.2) show the plot of the normalized amplitude of the input and output field of a straight waveguide. The overlap is calculated by storing all the temporal field values of E_y component for both the input and output field. Then they are Fourier transformed and the overlap is calculated. The waveguide parameters are $1.55\mu m$, $3\mu m$, $1\mu m$, $5\mu m$, $5\mu m$ for the wavelength, the refractive index of the waveguide, the background refractive index, the x-section and z-section of the computational window, respectively. In the first figure the length of the smoothed profile is 5 points while it is 10 points for the second figure. The smoothing technique is explained in details in [**?**].

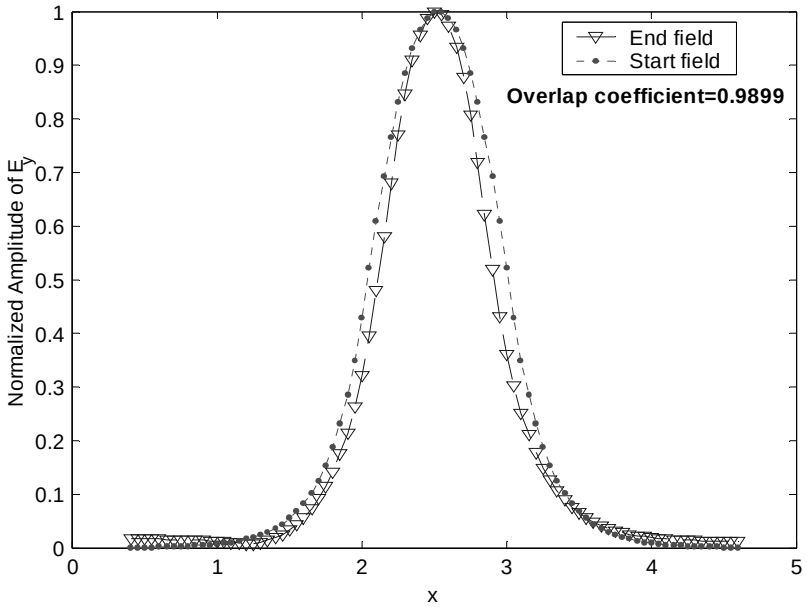

Fig.(6.1) Start and end field of a waveguide simulation, short smooth profile.

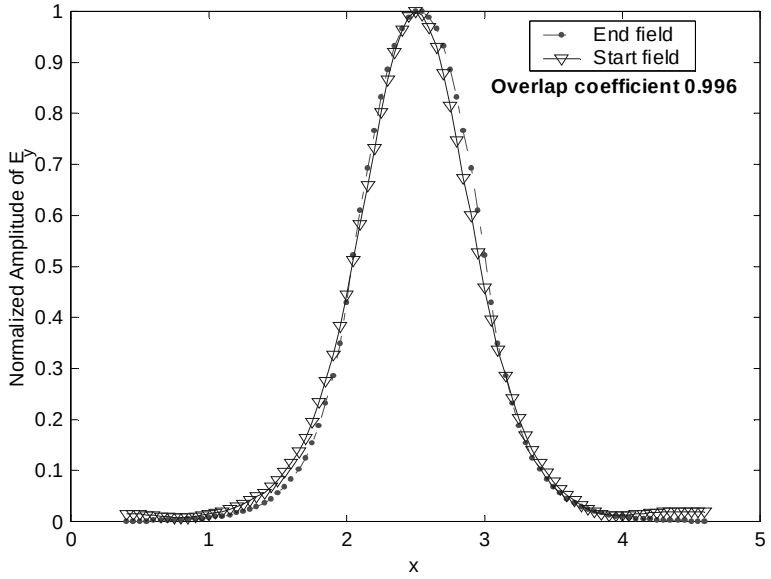

Fig.(6.2) Fig.(6.1) Start and end field of a waveguide simulation, long smooth profile.

Although the effect of smoothing is clear from the results shown in the previous figures, still investigating the effect of smoothing on the overall accurcy of the FDTD schemes was not considered due to time constrain and was left for futrue work.

6.2 Directional Coupler

Fig.(6.3) shows the intensity plot of the E_y field for a directional coupler of length 75 μm,this is also the length of the compuational window, width 1 μm and separation 1 μm. The wavelength was 5 μm, smaller wavelengths require long waveguides which means a huge number of grid points, and the width of the computational window in the x-direction was 10 μm. The step size was 0.1 and 0.25 μm in the x- and z-directions, respectively. The theoretical coupling length is 20.6303 μm and the numerical one is 20.62143 μm.

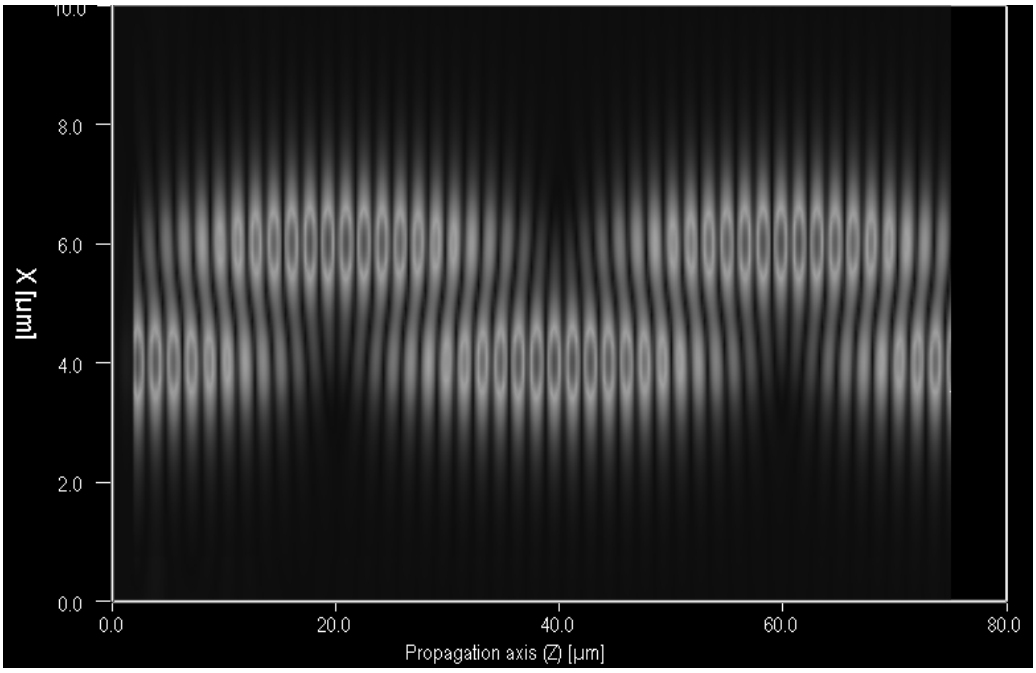

Fig.(6.3) The intensity plot of the E_y field component for a directional coupler.

Fig.(6.4) is the plot E_y field for the same structure simulated using beam propagation algorithm (BPM) implemented in the Promthesus program of Kymata.

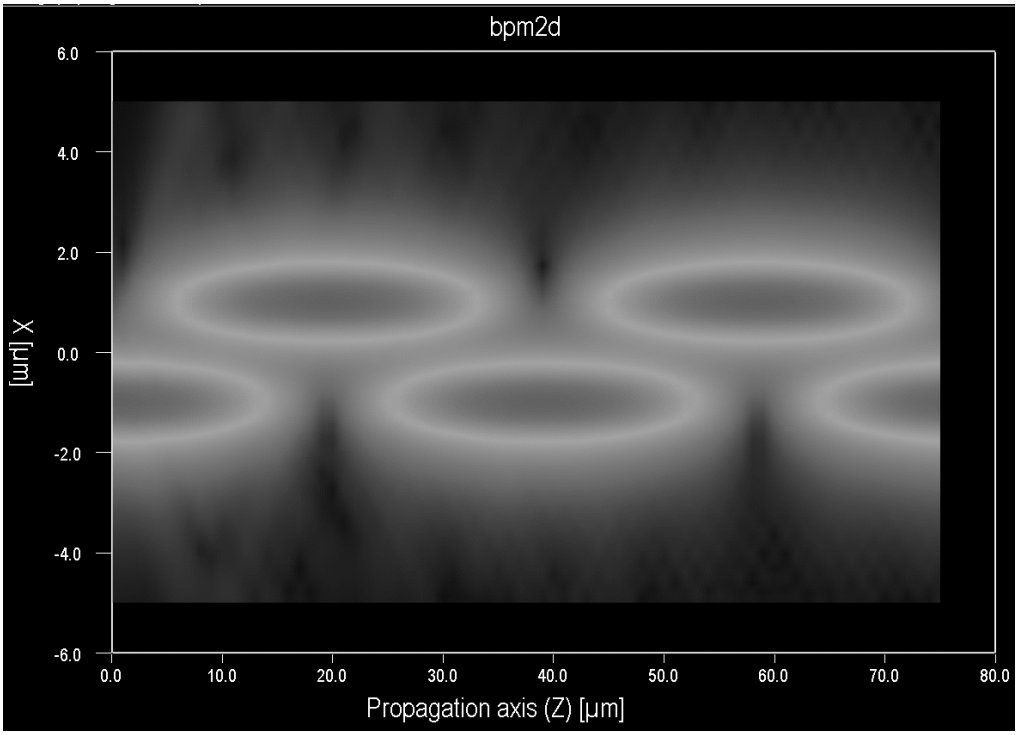

Fig.(6.4) The intensity plot of E_y field caculated using Promthesus program of Kymata software.

6.3 Conclusion

We quickly used our developed FDTD simulation tool to simulate a number of integrated optics devices. In the near future the performance of this tool will be analyzed in detail after implementing the needed post-processing tools.

Chapter 7

Conclusions and Recommendations

This chapter draws conclusions and suggest recommendations for future research based on our work with the FDTD that is presented in the previous chapters.

Before going into details discussion, I would like first to describe the status of my work and then possible future continuation and modification. At the end of this project I have implemented both the Yee(2,2) and Implicit(2,4) schemes in **2D** with PML-ABCs and TF/SF excitation. The exact index profiles are smoothed, when necessary, when mapped into the Yee grid. The implementation of these schemes was included in the Prometheus program of Kymata Netherlands software. This software environment enabled me to benefit from the graphical user interface as well as to access many integrated optics user defined functions and algorithms that increased the quality of this work. Still to be done, due to time limitations, is the implementation of many required post-processing tools that can be used to analyze the simulated structures.

In chapter two we presented the normalized Maxwell equations and we stated reasons for working with the normalized form. The normalization was extended to include the PML-ABCs parameters. In my opinion only in [**?**] for free space problems and in this work for waveguide problems, this normalized form was used when numerically solving Maxwell equations.

In chapter three we analyzed different FDTD schemes, the original one and higher order ones. Applying these schemes to free space problems in **1D** showed that the Implicit(2,4) does not introduce much improvement due to the additional computational cost required when using it. Therefore our first conclusion is not to consider it for further investigation. It was clear from the results presented in this work that the Explicit(2,4) scheme yeilds an improvement when compared to the Yee(2,2) scheme, however, it did not lead to a true fourth order approximation for realistic waveguide problems, even with different smoothed profiles.

On the other hand it is not staightforward to implement a truly fourth order scheme that can be applied to general or real life problems. It is worthwhile to implement a truly fourth order scheme [**?**] and compare with respect to the improvement and overhead to our Explicit(2,4)/Yee(2,2) scheme in **2D**.

In chapter four we presented two equivalent PML formulations, Berenger PML and unsplit PML. Although we did not consider any frequency-dependent materials, for which the unsplit formulation is well suited, we did apply it to free space problems in **1D** and **2D** and it is clear that it involves additional computational requirements. For the conventional Berenger PML we showed how to extend the index profile into the PML regions to simulate the extension of waveguides into these regions. The optimal values for the PML parameters can be selected from the graphs provided in that chapter.

In chapter five we investigated different excitation techniques and implemented TF/SF formulation in **2D** and the rest for **1D**. We showed how two simultaneous simulations are run at the same time and how the TF/SF formulation is implemented through combining fields from one simulation to the other. It is interesting to optimize this formulation by considering smaller structures or even a set of **1D** propagators in the simulation that is used to source the real desired simulation.

In my opinion all these techniques, except the transparent excitation in **2D** waveguide problems that was not investigated, offer good but not optimal excitation and need to be investigated more in future work especially the combination of the TF/SF formulation and the Implicit(2,4) scheme. Among these techniques, the TF/SF formulation seems to be the optimal one.

Generally speaking, working with **1D** FDTD problems was worthy for testing different schemes, PML-ABCs as well as excitation techniques. Only treating material interfaces was not fully clear in **1D** neither it is still in **1D**.

For the future, I am very interested in investigating wavelets time domain as well as finite element time domain method for simple **2D** structures and then comparing their performance with what I did in this work.

Acknowledgement 1 *I am very grateful to my supervisors Manfred Lohmeyer and Jan Bos for their continues support before and during the period of my final project. I must thank all staff members and teachers of the MSc program at faculty of Mathematical Sciences, Twente university with whom I work and enjoyed my two year MSc program. Special thanks to prof. Brenny van Groesen, prof. J. van der Vegt, prof. B. Geurts, dr. D. Dijkstra, dr. B. van de Fliert, dr. F. van Beckum, dr. S. van Gils, H. Margaretha and A. Suryanto. Special thanks to dr. R. Stoffer for his kindly support and useful discussion. I should also thank all the staff memebers of the LDG group at Twente university and specifically dr. H. Hoekstra and prof. P. Lampeck, and dr. R. de Ridder. I would also thank all the employees of Kymata Netherlands company with whom I spend more than half a year during my final project period. I am very grateful to H. Bulthius the Kyama's design manager for being a good co-supervisor and in many times a personal advisor for my future plans. Thanks go to Arien Bakker, Kymata's software manager. I do learned a lot from him and I appreciate his patient in facilitating my mission to work with the delict software of Kymata. Many thanks to all my colleges in the MSc. Special thanks to Emad Imreizeeq with whom I stayed for two years and I still have difficulties in writing his family name. Thanks for the only two Egyptians in Twente university Wael Hassan and Tarek El-Mansoury. Thanks to the Nuffic organization and the Nuffic employees for choosing me to be offered one of their many fellowships.*

Next,I must thank my family, especially my mother and my grand mother, all my brothers, and sisters and the rest of my bigger family in Alexandria, Egypt. Thanks to all my friends in Egypt for being so close to me during my first experience abroad and for their daily mails. Thanks to Ashraf said, Ali Attia, Muhummad El-Sayed, Ahmed Sherif, Islam El-Kabany, Yasser Fouad, and all my colleges at department of Mathematics, Faculty of Science ,Alexandria university. I would like also to thanks my Egyptian supervisors dr. Amr Elbakry and dr. Mahmoud El-alem. Special thanks to dr. Abdel-Hamid Ibrahim for his continuous concern about me and my future plans.

Finally, I am very grateful to the dutch society represented in all residential people of the small city of Enschede for being so wonderful and kind people during my first experience outside my country.